DNA-TR-84-54

INVESTIGATION OF ENVIRONMENT AND RESPONSE PHENOMENA FOR BURIED TARGET STRUCTURES IN CRATER MARGINS

Y. Marvin Ito
Russell H. England
Kenneth N. Kreyenhagen
California Research and Technology, Inc.
20943 Devonshire Street
Chatsworth, CA 91311-2376

1 May 1981

Technical Report

CONTRACT No. DNA 001-80-C-0168

THIS WORK WAS SPONSORED BY THE DEFENSE NUCLEAR AGENCY
UNDER RDT&E RMSS CODE B344080464 Y99QAXSC21038 H2590D.

Prepared for
Director
DEFENSE NUCLEAR AGENCY
Washington, DC 20305-1000

Destroy this report when it is no longer needed. Do not return to sender.

PLEASE NOTIFY THE DEFENSE NUCLEAR AGENCY, ATTN: STTI, WASHINGTON, DC 20305-1000, IF YOUR ADDRESS IS INCORRECT, IF YOU WISH IT DELETED FROM THE DISTRIBUTION LIST, OR IF THE ADDRESSEE IS NO LONGER EMPLOYED BY YOUR ORGANIZATION.

UNCLASSIFIED
SECURITY CLASSIFICATION OF THIS PAGE

AD-A166032

REPORT DOCUMENTATION PAGE

1a. REPORT SECURITY CLASSIFICATION UNCLASSIFIED	1b. RESTRICTIVE MARKINGS
2a. SECURITY CLASSIFICATION AUTHORITY	3. DISTRIBUTION/AVAILABILITY OF REPORT Approved for public release; distribution is unlimited
2b. DECLASSIFICATION/DOWNGRADING SCHEDULE N/A since UNCLASSIFIED	
4. PERFORMING ORGANIZATION REPORT NUMBER(S) CRT 3400F	5. MONITORING ORGANIZATION REPORT NUMBER(S) DNA-TR-84-54
6a. NAME OF PERFORMING ORGANIZATION California Research & Technology, Inc. — 6b. OFFICE SYMBOL (If applicable)	7a. NAME OF MONITORING ORGANIZATION Director Defense Nuclear Agency
6c. ADDRESS (City, State, and ZIP Code) 20943 Devonshire Street Chatsworth, CA 91311-2376	7b. ADDRESS (City, State, and ZIP Code) Washington, DC 20305-1000
8a. NAME OF FUNDING/SPONSORING ORGANIZATION — 8b. OFFICE SYMBOL (If applicable)	9. PROCUREMENT INSTRUMENT IDENTIFICATION NUMBER DNA 001-80-C-0168
8c. ADDRESS (City, State, and ZIP Code)	10. SOURCE OF FUNDING NUMBERS PROGRAM ELEMENT NO. 62715F — PROJECT NO. Y99QAXS — TASK NO. C — WORK UNIT ACCESSION NO. DH004775

There are situations in which peak overpressure on the surface may be a—

11. TITLE (Include Security Classification)
INVESTIGATION OF ENVIRONMENT AND RESPONSE PHENOMENA FOR BURIED TARGET STRUCTURES IN CRATER MARGINS

12. PERSONAL AUTHOR(S)
Ito, Y. Marvin; England, Russell H.; Kreyenhagen, Kenneth N.

13a. TYPE OF REPORT	13b. TIME COVERED	14. DATE OF REPORT (Year, Month, Day)	15. PAGE COUNT
Technical Report	FROM 800219 TO 810415	810501	120

16. SUPPLEMENTARY NOTATION
This work was sponsored by the Defense Nuclear Agency under RDT&E RMSS Code B344080464 Y99QAXSC21038 H2590D.

17. COSATI CODES			18. SUBJECT TERMS (Continue on reverse if necessary and identify by block number)
FIELD	GROUP	SUB-GROUP	
19	4		Cratering & Combined Effects (CARE) — Buried Structures
13	13		Finite-Element Models — Numerical Simulation

19. ABSTRACT (Continue on reverse if necessary and identify by block number)

Peak overpressure on the surface is widely used as the kill criterion in targeting studies. There are situations, however, in which this may be overly conservative or even a misleading kill criterion. ~~In particular,~~ to kill structures which are hardened to withstand the effects of several thousand psi overpressures may require such small miss distances for an ~~air~~blast-only kill that the structure will be within or very near the crater. ~~In such locations,~~ other effects - notably direct ground shock and cratering action become substantial, if not overwhelming, factors in the structure kill. (will then) (over)

In order to contribute to a more complete understanding of the response of buried structures near craters, an exploratory investigation was performed involving the following approach:

1. Review experimental data for model structures exposed to the near-crater (over)

20. DISTRIBUTION/AVAILABILITY OF ABSTRACT	21. ABSTRACT SECURITY CLASSIFICATION
☐ UNCLASSIFIED/UNLIMITED ☒ SAME AS RPT. ☐ DTIC USERS	UNCLASSIFIED
22a. NAME OF RESPONSIBLE INDIVIDUAL Betty L. Fox	22b. TELEPHONE (Include Area Code) (202) 325-7042 — 22c. OFFICE SYMBOL DNA/STTI

DD FORM 1473, 84 MAR — 83 APR edition may be used until exhausted. All other editions are obsolete.

SECURITY CLASSIFICATION OF THIS PAGE
UNCLASSIFIED

20. Abstract (continued)

environment in high-explosive (HE) tests.

2. Define free-field dynamic crater environment, starting with an HE event (MIDDLE GUST III), using results of a recently completed numerical simulation.

3. Develop simplified methodology for determining structure-media interactions in the grossly-deforming near crater environment.

4. Evaluate response and vulnerability of representative buried structures exposed to near-crater environment.

Based on the results of this exploratory investigation, the following conclusions are drawn:

- Using simulated MIDDLE GUST III dynamic environment, response of representative structures at various ranges near the crater ~~has been~~ analyzed ~~using simplified models~~. For example, the MX-B vertical shelter ($\ell/d = 7$) is predicted to be destroyed in the crater margin due to decoupled effects of peak ground shock pressure (crushing), dynamic ground shock gradient (plastic hinge), and late-time differential displacement (plastic hinge).
- Distinct layering in the MIDDLE GUST III geology (probably typical of many target sites) substantially affects structure vulnerability to dynamic ground shock gradient and late-time differential displacement from cratering flow.
- Environment near nuclear craters will be more severe than near HE craters, due to effects of 5-10 times higher peak overpressure at crater radius. Thus, HE sources alone will not simulate the combined environment effects near nuclear craters.
- If test sites which are chosen have no strong reflective interface at a relatively shallow depth, the near-crater environment for model structures will probably not be as severe as for full-scale structures near nuclear craters in typical layered geologies.

SUMMARY

The technologies of cratering, ground motions and non-linear structural response have been brought together to develop and apply a simplified methodology for analyzing the response of structures in the grossly-deforming crater-margin environment. The effort has resulted in initial steps towards identifying and quantifying major kill mechanisms in this combined effects environment.

DEFINITION OF NEAR-CRATER ENVIRONMENT

Numerical cratering solutions provide the only current means for complete description of the dynamic environment near craters. They provide stress and displacement histories of the near-crater environment which can be used to evaluate the vulnerability of structures.

Experimental data primarily consist of permanent displacements from sand columns. HE data has been reviewed and correlated with scaled slant range in different tests and media. Data scatter is very large, about a factor of four in weak soils.

The detailed definition of the free-field crater environment from a recently completed numerical calculation of the MIDDLE GUST III HE event has been used in the current investigation. The peak compressive stress contours for MIDDLE GUST III show an important characteristic of this layered geology, namely the rapid attenuation which occurs in the more dissipative shallow soil layers above the rock layers. Thus, shallow-buried

structures may be subjected to a less severe direct-induced stress environment than deeper structures in the rock layers. Also, a sharp displacement gradient occurs at the soil/rock interface.

VULNERABILITY OF STRUCTURES NEAR CRATERS

Simplified soil/structure interaction methods have been developed to evaluate the response of structures in the near-crater environment. These techniques are used to examine the separate effects of peak ground shock, dynamic ground shock gradient and cratering flow displacement.

Failure due to Peak Ground Shock:

A finite-element soil/structure analysis was used to evaluate the relationship between free-field stress and soil/structure interface stress. Given this relationship, static collapse analysis was used to determine structural vulnerability due to ground shock.

In the MIDDLE GUST III near-surface wet geology, the peak interface stress was found to be essentially the same as the peak free-field stress. Thus, the predicted collapse contours for typical structural cross-sections are determined using the peak ground shock pressure.

Failure due to Dynamic Ground Shock Gradient:

The early-time bending response of structures is excited by the temporal and spatial gradient of the ground shock along the structure length. A finite-element analysis of soil/structure

interaction showed that structures are initially accelerated with the free-field ground shock motion. Thus, the free-field ground shock motion was used to define the early-time dynamic loading on the structure.

Finite-element beam (2-D plane stress) models were used to evaluate the early-time bending response of vertical shelters and silos placed in the simulated MIDDLE GUST III dynamic ground shock gradient. The maximum predicted range for destruction of these vertical structures are in the crater margin.

Failure due to Cratering Flow Displacement:

The late-time bending response of structures was evaluated using a quasi-static finite-element beam analysis procedure with non-linear soil springs to account for the soil/structure interaction loads which occur during cratering flow.

The response of shelters and silos was considered for the MIDDLE GUST III geology (wet clay over weathered shale), using the calculated free-field crater flow displacement. These results show a substantial drop in peak bending stress near the crater edge and the significant effect of the clay/shale interface.

CONCLUSIONS

Based on the results of this exploratory program the following conclusions are drawn:

- Using simulated MIDDLE GUST III dynamic environment, response of representative structures (MX-B shelter and STP silo) at various ranges has been analyzed using

structural engineering models. These structures are predicted to be destroyed out to the following maximum ranges due to the decoupled effects of:

Environment (Failure)	MX-B	STP
peak ground shock pressure (crushing)	55 ft	50 ft
dynamic ground shock gradient (plastic hinge)	58 ft	50 ft
late-time differential displacement (plastic hinge)	55 ft	<30 ft

These ranges are all in the crater margin where the crater radius is at 55 ft.

- Distinct layering in the MIDDLE GUST III geology (probably typical of many target sites) substantially affects structure vulnerability to dynamic ground shock gradient and late-time differential displacement from cratering flow.

- Environment near nuclear craters will be more severe than near HE craters, due to effects of 5-10 times higher peak overpressure at crater radius. Thus, HE sources alone (hemisphere of TNT or capped cylinder of ANFO) will not simulate the combined environment effects near nuclear craters.

- If test sites which are chosen have no strong reflective interface at a relatively shallow depth, the near-crater environment for model structures will probably not be as severe as for full-scale structures near nuclear craters in typical layered geologies.

- For structures testing, it would be desirable to select sites with representative scaled layering, and to field structure models both entirely within layers, and extending between layers.

PREFACE

This final report describes (primarily in briefing format) an exploratory investigation of environment and response phenomena for buried target structures in crater margins. The investigation was performed for the Defense Nuclear Agency (DNA) under Contract DNA001-80-C-0168. The DNA technical monitors were Dr. Kent L. Goering and Maj. Myron E. Furbee.

The authors have received valuable assistance from many discussions with D. L. Orphal, S. Schuster, M. H. Wagner and Prof. R. B. Nelson. In addition, Y. Muki and F. W. Ross-Perry provided assistance in the performance of the numerical calculations.

CONVERSION FACTORS

To Convert From	To Metric (SI) Units	Multiply By
degree (angle)	radian (rad)	1.745 x E -2
foot	meter (m)	3.048 x E -1
inch	meter (m)	2.540 x E -2
pound-force (lbf avoirdupois)	newton (N)	4.448
kip (1000 lbf)	newton (N)	4.448 x E -3
pound-force/inch^2 (psi)	kilo pascal (kPa)	6.894
kip/inch^2 (ksi)	kilo pascal (kPa)	6.894 x E -3
ton (t)	megajoule (MJ)	4.183 x E +3
kiloton (kt)	megajoule (MJ)	4.183

A more complete listing of conversions may be found in "Metric Practice Guide E 380-74", American Society for Testing Materials.

TABLE OF CONTENTS

LIST OF ILLUSTRATIONS

LIST OF ILLUSTRATIONS (continued)

LIST OF ILLUSTRATIONS (Continued)

LIST OF TABLES

SECTION 1

INTRODUCTION

1.1 BACKGROUND

Peak overpressure (ΔP_{max}) on the surface is widely used as the kill criterion in targeting studies. This is because ΔP_{max} is applicable to both HOB and contact bursts, and because it is predictable with some confidence, and because it is largely independent of target media. There are situations, however, in which ΔP_{max} is overly conservative or even a misleading kill criterion. In particular, to kill structures which are hardened to withstand the effects of several thousand psi overpressures may require such small miss distances for an airblast-only kill that the structure will be within or very near the crater. In such locations, other effects - notably direct ground shock and cratering action - become substantial, if not overwhelming factors in the structure kill.

Instinctively, one believes that any practical military structure which is close enough to a burst to be within the actual crater or even in the grossly-deformed region immediately surrounding that crater will be convincingly destroyed by the severe combined effects of direct ground shock, airblast-induced ground shock, and large local gradients in displacements. However, in a recent near-surface burst test [1] have in which model structures were buried near the expected edge of craters (i.e., in the region we will refer to as the "crater margin"), the model structures survived even though they were ejected from the crater.

1.2 OBJECTIVES

The rather surprising results of these observations for model structures near HE craters indicate a need for more complete understanding of the response of buried structures near craters. It is the overall objective of this investigation to contribute to such understanding through:

- Definition of the nature of the dynamic environment within the margins of craters formed by near-surface bursts over various generic media, and
- Examination of the response and vulnerability of generic structures in that environment.

1.3 APPROACH

Within this overall objective, the investigation consisted of the following tasks:

1) Review of experimental data for model structures exposed to the near-crater environment in HE tests.
2) Detailed definition of free-field dynamic crater environments, starting with an HE event (MIDDLE GUST III), using results of a recently-completed numerical calculation on another contract (DNA001-80-C-0265).
3) Development of simplified methodology for defining structure-media interactions in the grossly-deforming near-crater environment.
4) Evaluation of response and vulnerability of representative buried structures exposed to near-crater environment.

SECTION 2

OVERPRESSURE AT CRATER RADIUS

This section gives the peak overpressure at the crater radius in various media and a comparison of simple-geometry high-explosive (HE) and nuclear (NE) bursts. It is noted that the environment near nuclear craters will be more severe than near HE craters, due to effects of 5-10 times higher peak overpressure at crater radius. Thus, simple-geometry HE sources alone do not simulate the combined environment effects near nuclear craters.

- Table 1 summarizes experimental data [2,3,4] from near-surface nuclear cratering events. The final column is the peak overpressure at the measured crater radius, as predicted by the Brode relationship. All events were at the Pacific Proving Grounds in coral, except for JOHNIE BOY and JANGLE S which were at the Nevada Test Site in alluvium. Note that with the exception of ZUNI, all the high-yield shots have relatively low overpressures at the crater edge.

Table 1. Crater Parameters For Near-Surface Nuclear Test Events [2,3,4]

Event	Yield (kT)	HOB (ft)	SHOB ($ft/kT^{1/3}$)	Medium	Scaled Crater Volume, V/W (ft^3/Ton)	Crater Radius (ft)	Scaled Radius ($ft/kT^{1/3}$)	Brode Peak Overpressure at Crater Radius (ksi)
IVY MIKE	10,400	10	0.5	PPG	110	2910	133	1.5
CASTLE BRAVO	15,000	7	0.3	PPG	125	3255	132	1.5
CASTLE KOON	150	9.3	1.8	PPG	88	495	93	4.5
CACTUS	18	3	1.1	PPG	102	174	66	12.0
OAK	9,000	6.5	0.3	PPG	189	2870	138	1.4
KOA	1,300	3	0.3	PPG	499	2159	198	0.6
ZUNI	3,400	9.6	0.6	PPG	55	1165	77	7.5
TEWA	4,600	12.3	0.7	PPG	149	1916	115	2.5
LACROSSE	39.5	8	2.3	PPG	72	200	59	16.9
SEMINOLE	13.7	7	2.9	PPG	470	325	136	1.5
JOHNIE BOY	0.5	-1.75	-2.2	Alluvium	280	61	77	7.1
JANGLE S	1.2	3.5	3.3	Alluvium	37	45	42	56.4

- Best-estimate nuclear surface contact burst cratering parameters for generic media are shown in Table 2 from Cooper [5]. Corresponding peak overpressures at the crater edge are indicated in the last column.

Table 2. Nuclear Contact Burst - Cratering Parameters for Generic Materials [5]

Medium	Crater Volume (ft^3/kT)	Crater Radius ($ft/kT^{1/3}$)	Brode Overpressure at Crater Radius (ksi)
Coral	200,000	75 - 150	7 - 1
Wet Soil	200,000	64 - 82	13 - 6
Wet Soft Rock	100,000	51 - 65	29 - 22
Dry Soil	50,000	41 - 52	63 - 27
Soft Rock	40,000	38 - 48	84 - 36
Hard Rock	25,000	32 - 41	159 - 63

- Best-estimate high-explosive surface tangent cratering parameters for generic media are given in Table 3 following Cooper [5]. As seen by comparison with Table 2, such HE sources are estimated to be five times more efficient in excavating crater volumes than NE contact bursts. This is one reason why the peak overpressure at the crater edge, as predicted by AFWL [4], is much smaller, as shown in the final column.

Table 3. HE Surface Tangent - Crater Parameters for Generic Materials [5]

Medium	Crater Volume (ft^3/kT)	Crater Radius ($ft/kT^{1/3}$)	AFWL Overpressure at Crater Radius (ksi)
Wet Soil	1,000,000	110 - 140	2.2 - 1.6
Wet Soft Rock	500,000	87 - 111	2.8 - 2.2
Dry Soil	250,000	69 - 88	3.5 - 2.8
Soft Rock	200,000	64 - 82	3.6 - 3.0
Hard Pock	125,000	55 - 70	4.0 - 3.4

- Figure 1 gives a comparison of the peak overpressure levels at the crater edge for nuclear and high-explosive events in various generic media based on Tables 2 and 3, and using an equivalence factor between HE surface tangent spheres and contact nuclear bursts of 5, i.e., $W_{HE} = 1/5\ W_N$. For example, Cooper [5] predicts an HE crater in wet soft rock will have a scaled radius between 51 and 65 ft/$KT_N^{1/3}$. The overpressures at these radii are 2.8 ksi and 2.2 ksi, respectively.

- Note that peak overpressures at the crater edge for nuclear events are factors of 5-10 higher than for HE events.

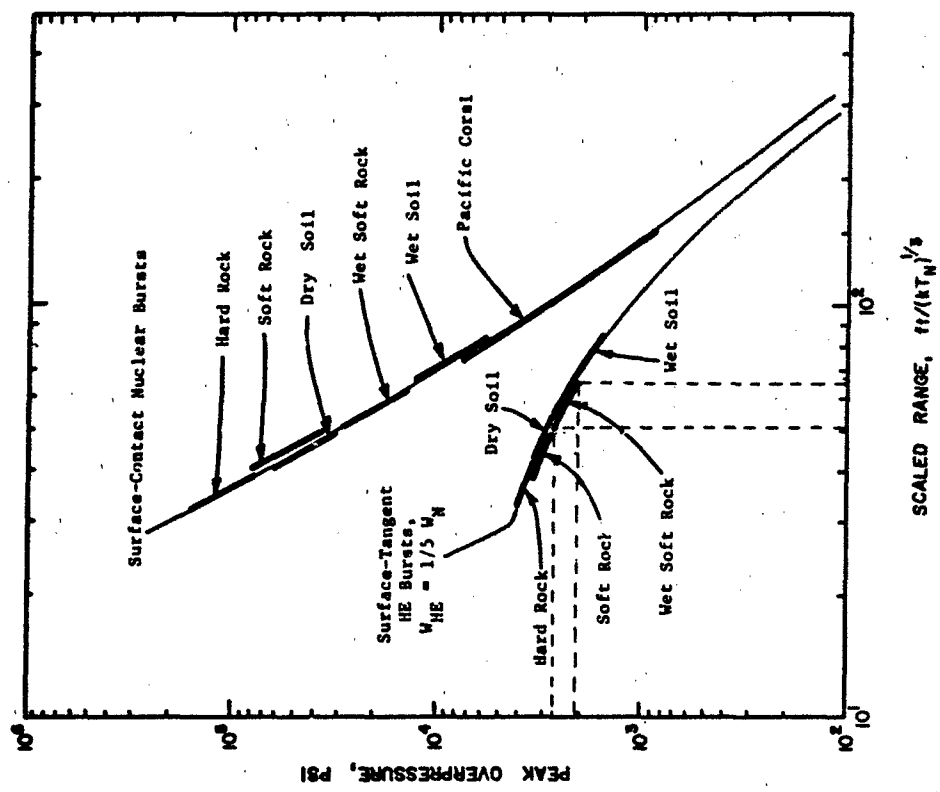

Figure 1. Peak Overpressures at Crater Radius in Different Media (For HE Bursts, Scaled Radius and Overpressure Assume $W_{HE} = 1/5\ W_N$).

SECTION 3

EXPERIMENTS WITH STRUCTURES NEAR CRATERS

Several high-explosive (HE) tests involving surface or near-surface explosions have been conducted to obtain data on the effects of nuclear weapons on various buried structures. Some of these results have indicated that even the severe environment within or near the edge of craters may not be sufficient to produce assured destruction of some hardened targets. In a recent test [1], reinforced concrete thin-walled box-type structures located near the surface in silty clay did not collapse, even though they were ejected from the crater of a buried charge.

This is perhaps an extreme example, and the military utility of a target structure which has been tossed about and totally disoriented is questionable, even though the integrity of the shell may not have been totally violated. On the other hand, such evidence raises doubts about any easy assumption in targeting studies that structures within craters are assuredly destroyed. In addition, not all such structures necessarily become part of the ejecta. Those especially which are in the crater rim or which impinge into the crater (even substantial distances) may not only survive but may also be only moderately disoriented.

This section gives a summary of the key tests with structures near craters. It is noted that most scaled-structure models were not exposed to the severe deformation which occur within craters.

- This figure summarizes structural response of the DUGWAY-403 test [6]. The thin wall reinforced concrete box structures were placed near the crater edge and received damage mostly caused by the ground shock pressure.

Test: DUGWAY-403 (Ref. 6)

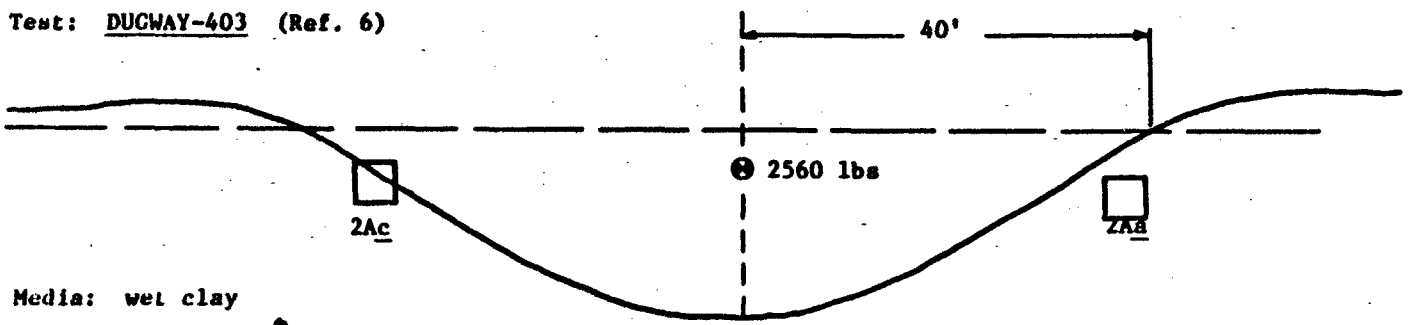

Media: wet clay

Structure	Type	Wall Thickness t_{min}	Span D	Length L	Range from Source	Depth to top	Peak Free Field Soil Pressure	Peak Interface Pressure	Response
2Aa	Box	5"	5'	5'	36'	3'	-	260 psi	Moderate tensile cracking occurring from ground shock pressures.
2Ac	Box	5"	5'	4'	32'	3'	-	-	Heavy tensile cracking and large structure motions caused by crater formation.

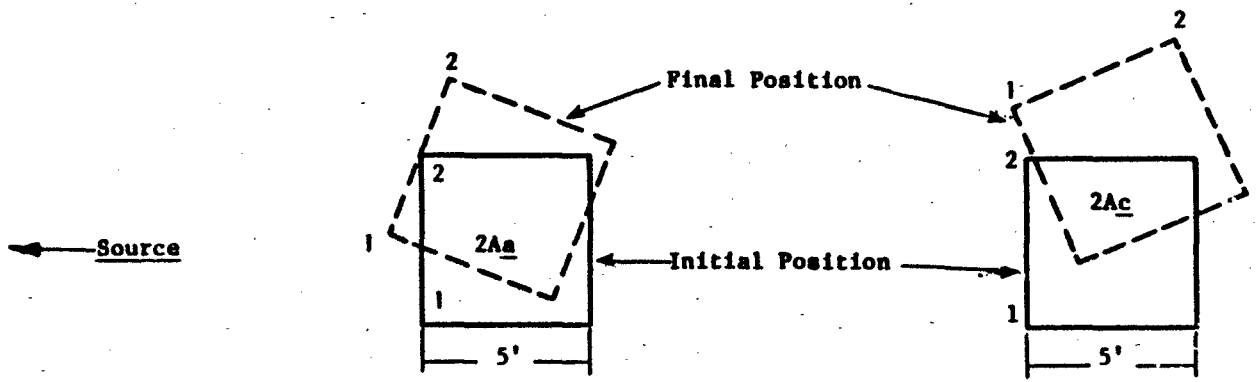

Figure 2. Structural Response from the DUGWAY-403 Test.

- This figure summarizes structural response of the ESSEX V hardened structure test [7]. The shock from free-field and interface pressures were relatively low and the structures experienced moderate rigid body motions associated with crater formation.

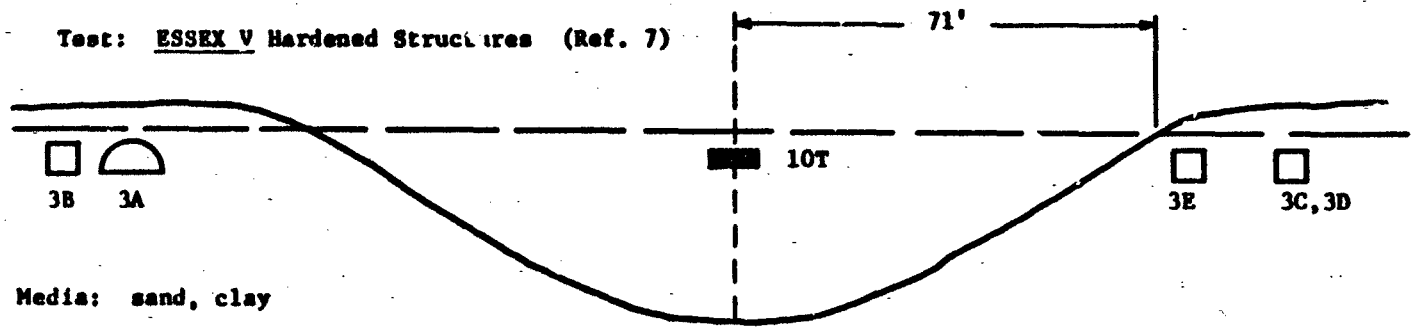

Structure	Type	Thickness t	Span D	Length L	Range	Depth	Peak Free Field Soil Pressure	Peak Interface Pressure	Response
3A	Arch	11.0"	15.8'	24.5'	92'	2'	40 psi	75 psi	Elastic
3B	Box	5.6"	4.9'	49.3'	105'	2'	40 psi	55 psi	Elastic
3C	Box	5.6"	4.9'	49.3'	92'	2'	50 psi	55 psi	Elastic
3D	Box	18.0"	6.2'	24.7'	92'	2'	40 psi	75 psi	Elastic
3E	Box	18.0"	6.2'	24.7'	72'	2'	100 psi	100 psi	Elastic

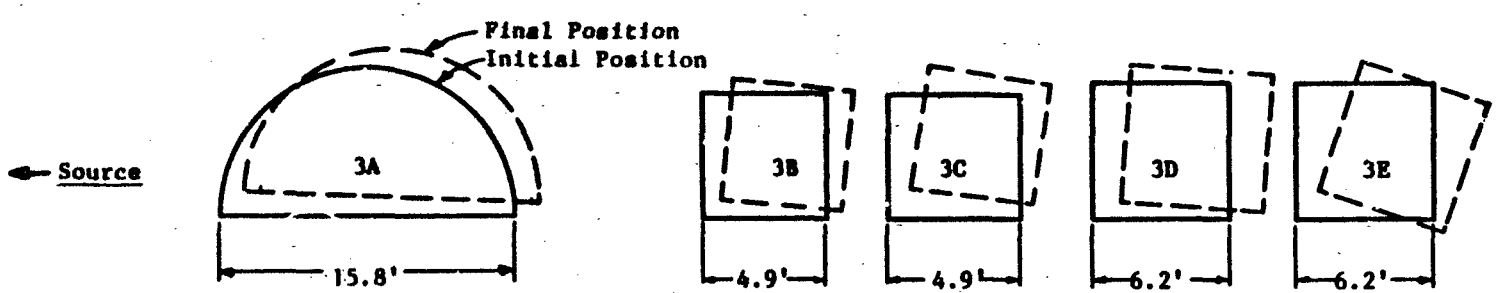

Figure 3. Structural Response from the ESSEX V Test.

- This figure summarizes structural response of the ESSEX I Phase 2 structure test [8]. The ground shock pressures at the range of the hardened box structures were low. However, the large gradient on displacements associated with crater formation caused bending failures of the complex structure. This was one of the few tests where very long structures were fielded.

Test: ESSEX I Phase 2 Structure Test (Ref. 8)

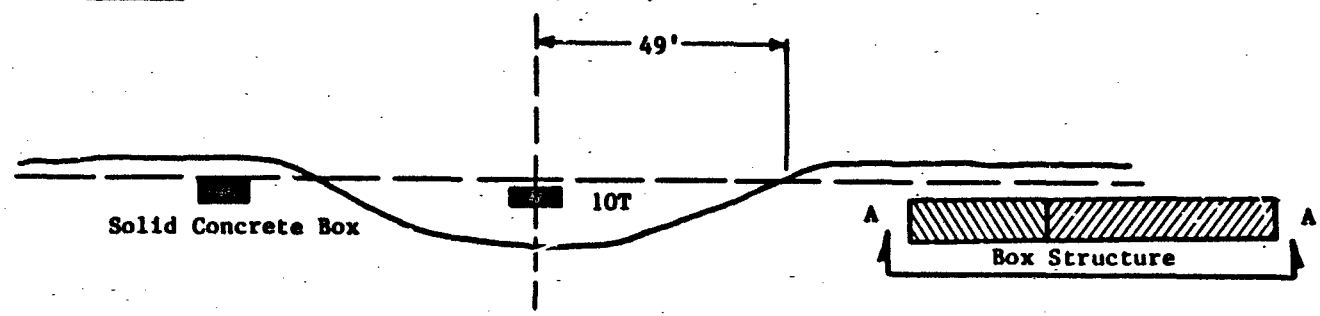

Media: sand, clay

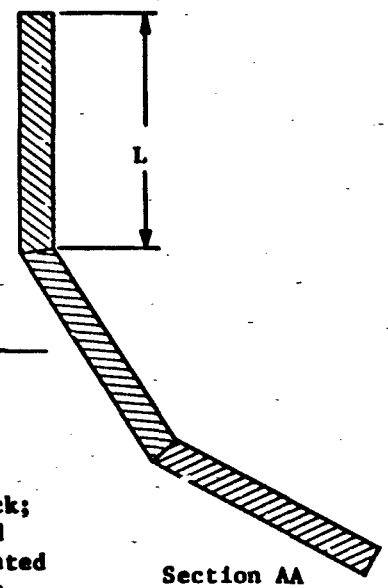

Structure	Thickness t	Span D	Length L	Range	Depth	Response
Solid Concrete Block	4'	10'	10'	65'	0	No structural damage
Box Structure	1'	6'	50'	75'	2'	No structural damage caused by ground shock; however, large scaled displacements associated with crater formation caused bending failures

Figure 4. Structural Response from the ESSEX I Phase 2 Test.

- This figure summarizes structural response of the TEA POT ESS Test [9]. The thin walled concrete box structures in this test remained elastic and experienced moderate rigid body motions.

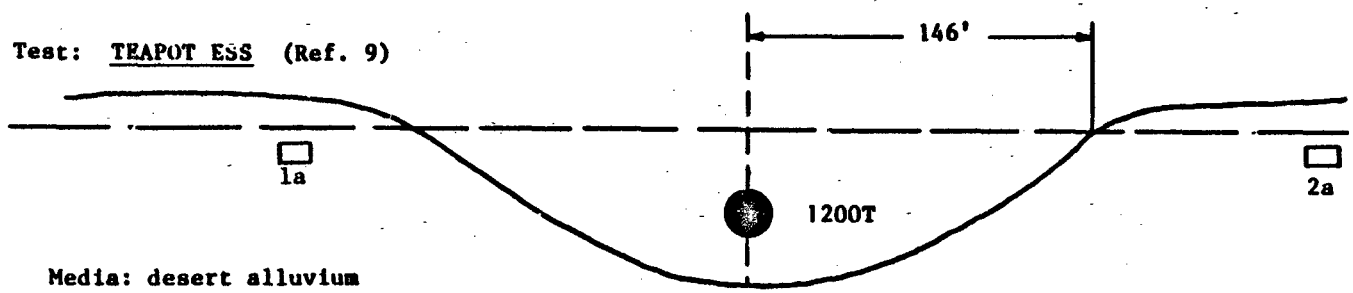

Structure	Type	Thickness t_{min}	Span D	Length L	Range	Depth	Peak Free Field Soil Pressure	Peak Interface Pressure	Response
1a	Box	12.5"	12.5'	12.5'	200'	3.75'	125 psi	40 psi	Elastic
2a	Box	12.5"	12.5'	12.5'	250'	3.75'	50 psi	50 psi	Elastic

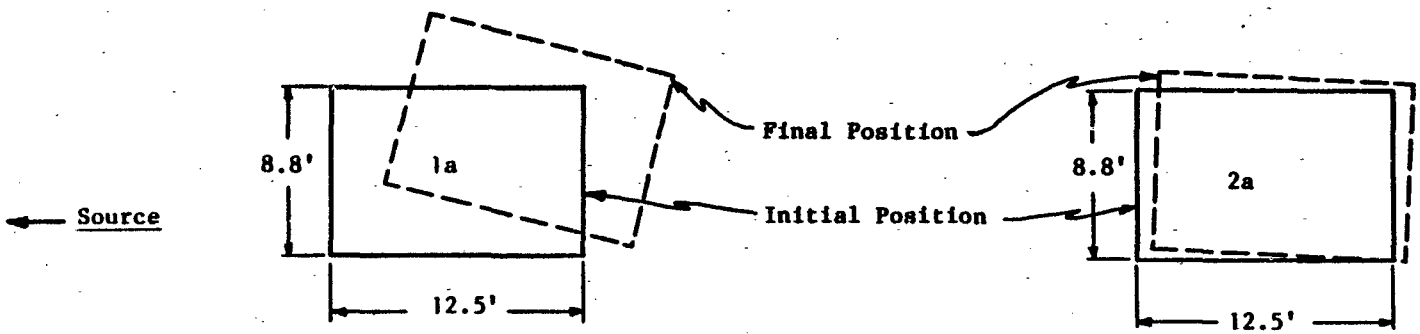

Figure 5. Structural Response from the TEAPOT ESS Test.

- This figure summarizes structural response of the Middle Gust III test [10,11]. In this test some of the steel cylinders placed inside the crater failed, whereas structures placed outside the crater remained elastic. The crater formation induced large rigid body structural motion especially near the crater.

Test: MIDDLE GUST III (Ref. 10, 11)

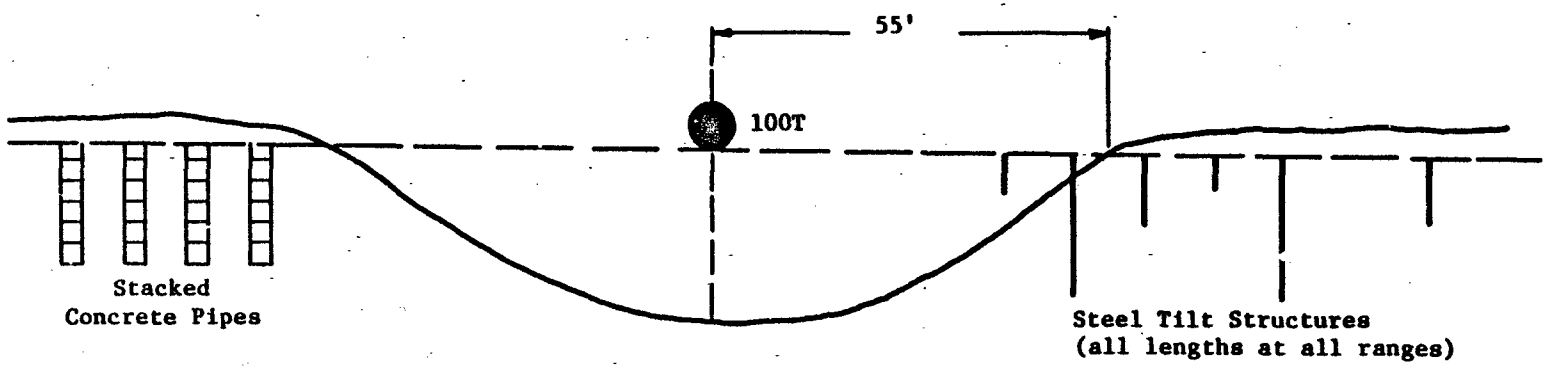

Media: wet clay/shale

Structure	Type	Thickness t	Diameter D	Length L	Range	Response
Tilt Gage	Cylinder	Thick Walled	6"	5', 9', 20'	42', 52', 72', 88' 110', 125', 165', 225'	Some of the steel tilt structures placed inside the crater survived. All structures placed outside were undamaged.
Concrete Pipes	Cylinder	8"	44"	36" per section 3 to 6 sections per cylinder	88', 110', 125'	The concrete structures in Middle Gust III remained essentially elastic, however the 3' sections of the concrete pipes separated. In an earlier test (Middle Gust II), the same concrete structures placed near the crater edge were destroyed. (Structures placed at 52 ft range, crater radius was 43 ft.)

Figure 6. Structural Response from the MIDDLE GUST III Test.

- This figure describes the structural response of the DIAL PACK test [12]. The structure, a scaled Minute Man reinforced concrete silo remained elastic.

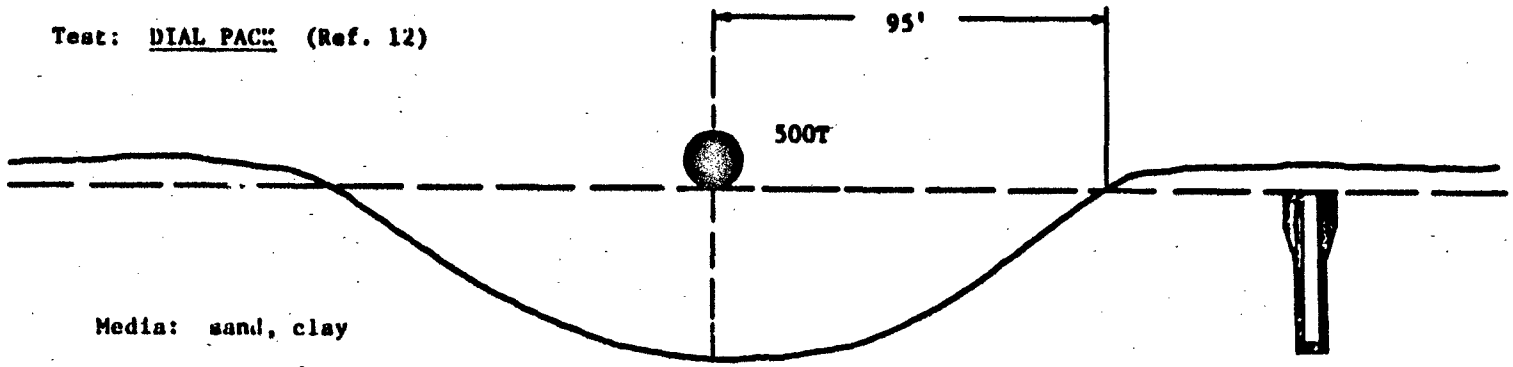

Structure	Type	t_{min} Thickness	D_{min} Diameter	L Length	Range	Depth	Response
Silo	Reinforced	1'	7.7'	43'	135'	Surface	Structure sustained no noticable damage. Structure was stressed to near yield by 850 psi peak overpressures. The stresses induced by the late-time formation of the crater are small, although crater induced motions are large compared to air blast. Peak silo displacements were 5 to 10 times greater than the permanent displacements.

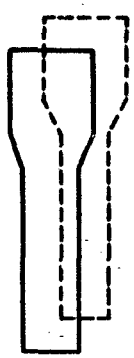

Peak Silo Displacement

Figure 7. Structural Response from the DIAL PACK Test.

- This figure summarizes the structural response of the MINERAL ROCK test [13,14]. The damage levels for structures fielded near the crater were high caused by the opening and sliding of existing rock joints.

Test: MINERAL ROCK (Ref. 13, 14)

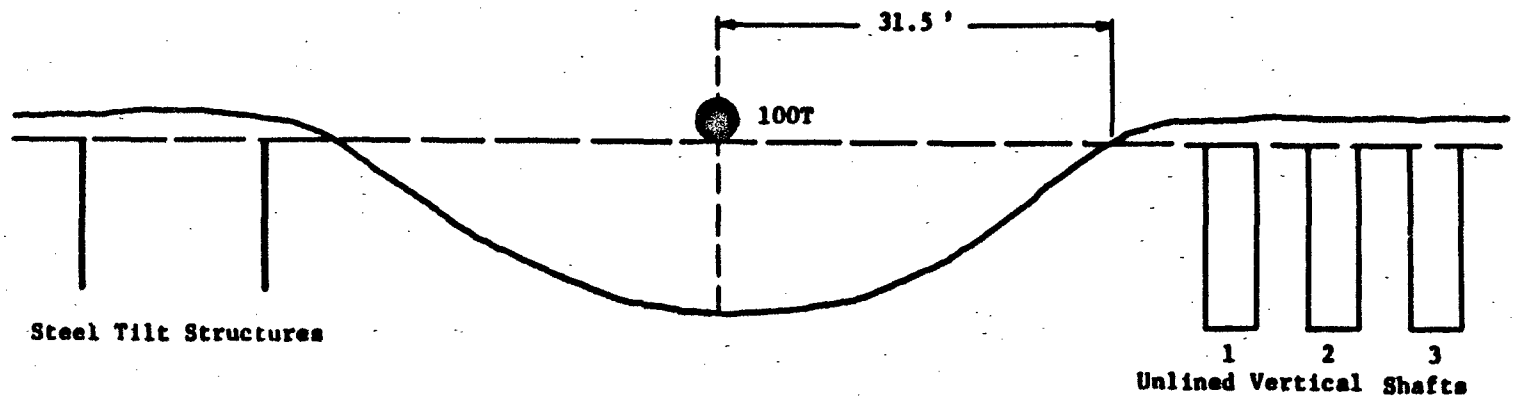

Media: quartz-diorite

Structure	Type	Diameter D	Length L	Range	Response
1	Unlined Shafts	56"	15'	40'	Significant crushing, cracking and permanent damage.
2	Unlined Shafts	56"	15'	50'	Significant cracking and permanent displacement, less crushing.
3	Unlined Shafts	56"	15'	60'	Moderate cracking, no crushing or permanent displacements.
Tilt	Thick Walled Steel Shafts	6"	10' 20'	35' 50' 80'	The tilt structures placed at 35' were essentially destroyed. Structures at 50' had considerable damage to the portion of pipe protruding above the rock surface, and some damage was observed at lower depth, possibly the result of a horizontal fracture plane in the granite. The tilt structures at 80' were undamaged except above the rock surface.

Figure 8. Structural Response from the MINERAL ROCK Test.

SECTION 4

DEFINITION OF NEAR-CRATER ENVIRONMENT

Numerical cratering solutions provide the only current means for complete description of the dynamic environment near craters. They provide stress and displacement histories of the near-crater environment which can be used to evaluate the vulnerability of structures.

Experimental data primarily consist of permanent displacements from sand columns. HE data has been reviewed and correlated with scaled slant range in different tests and media. Data scatter is very large, about a factor of four in weak soils.

The detailed definition of the free-field crater environment from a recently completed numerical calculation of the MIDDLE GUST III HE event has been used in the current investigation. The peak compressive stress contours for MIDDLE GUST III show an important characteristic of this layered geology, namely the rapid attenuation which occurs in the more dissipative shallow layers. Shallow-buried structures may therefore be subjected to a less severe environment than deeper structures in this geology. Also, a sharp displacement gradient occurs near the material interface.

4.1 Experimental Near-Crater Data

- Primarily consist of permanent displacements from sand columns in HE tests.
- Carnes [15] summarizes HE data and correlates with scaled slant range in different tests and media. Data scatter is very large, about a factor of four in weak soils.
- Data should be analyzed further.

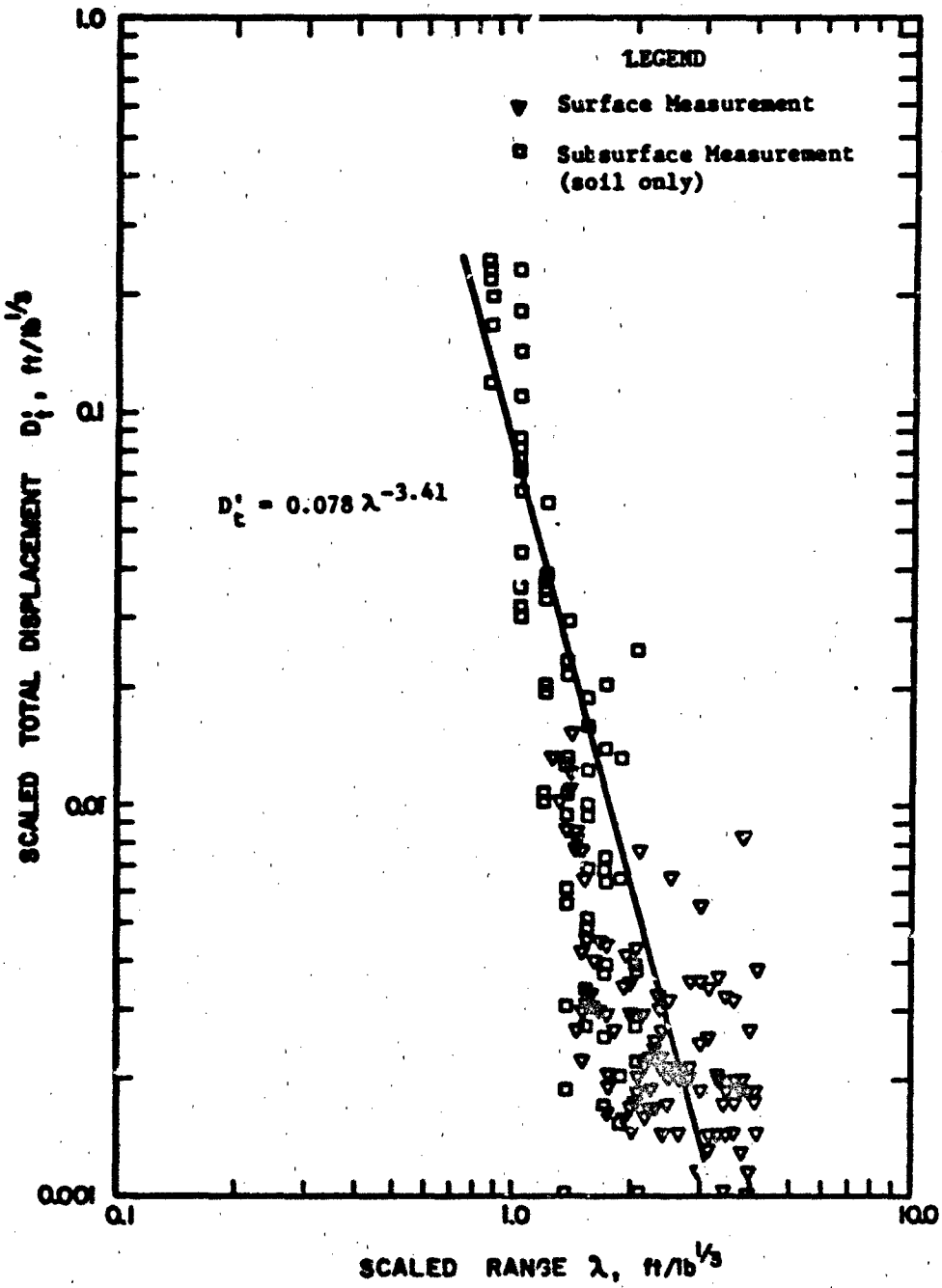

Figure 9. Permanent Displacements from Middle Gust Event 3. All Data Were Measured in the Soil at or near the Surface. (From Carnes, Ref. 15)

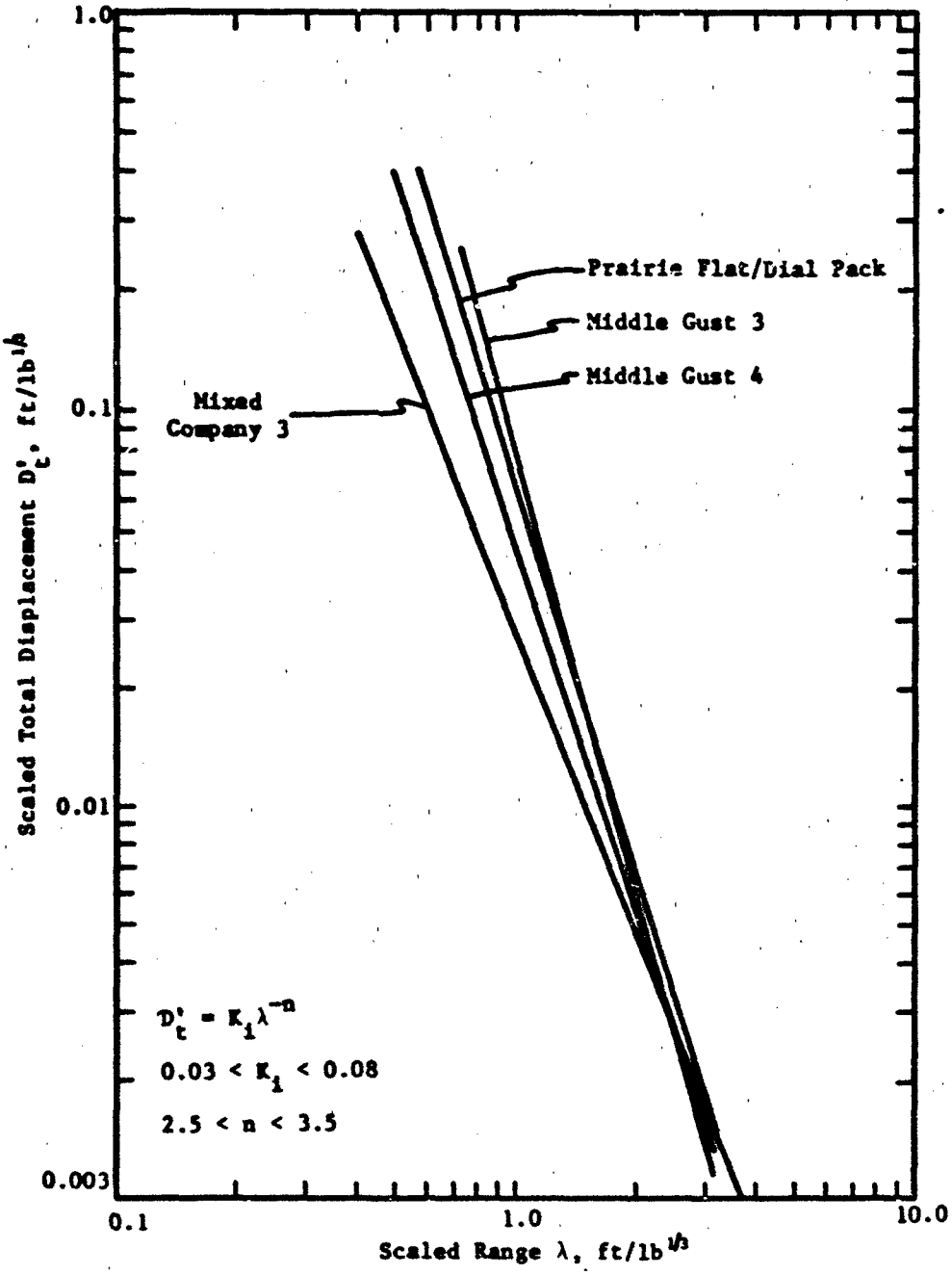

Figure 10. Range of permanent displacements in weak soil for surface tangent events. (Data scatter about a factor of four.) (From Carnes, Ref. 15)

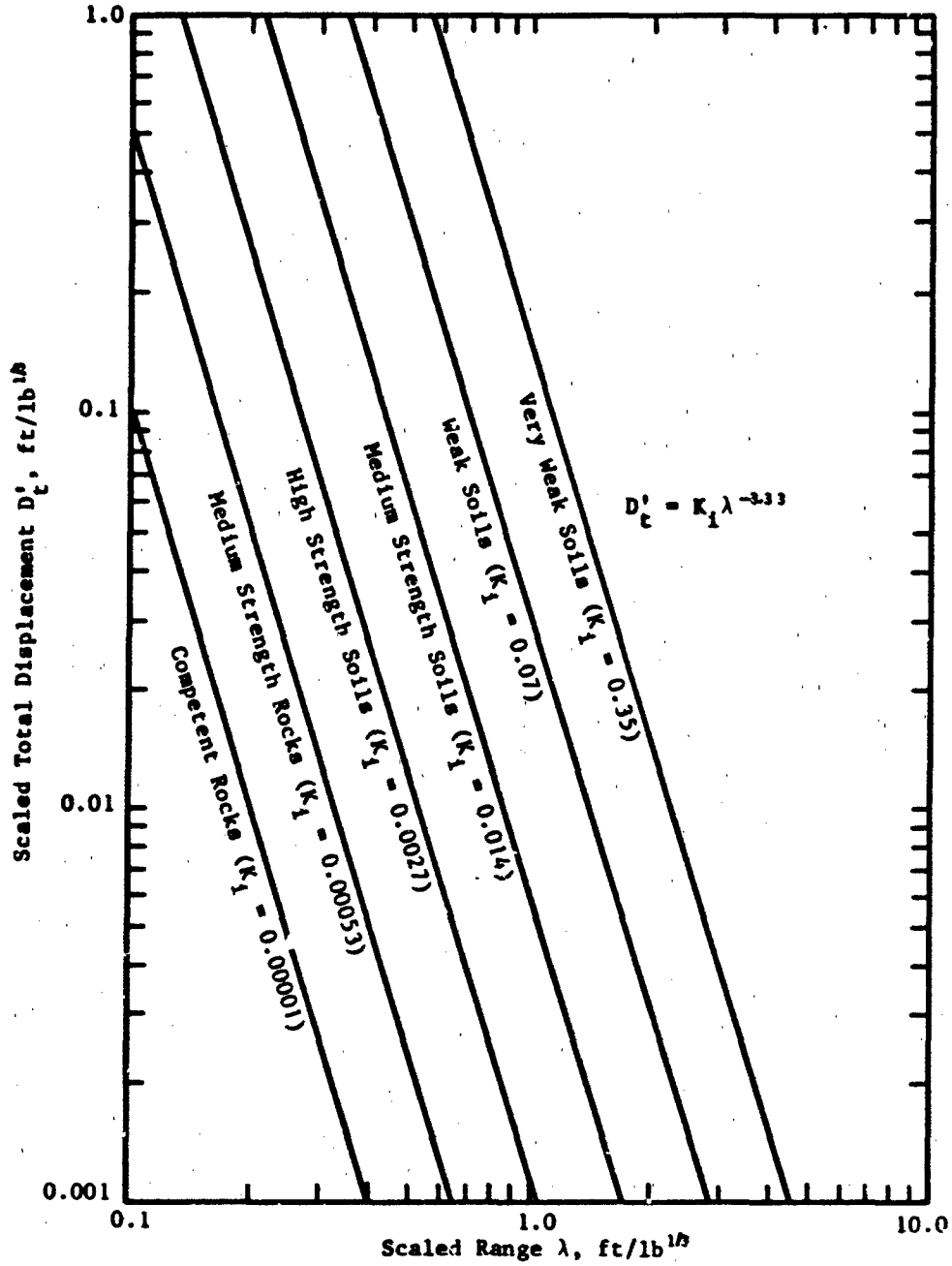

Figure 11. Range of permanent displacement for various geologic media for surface tangent and above surface charge geometries (K_1 is the value of D_ξ' at $\lambda = 1.0$). (From Carnes, Ref. 15)

4.2 Numerical Calculations of Nuclear Craters

- Numerical solutions provide only current tool for complete description of dynamic environment near craters.

- Five major calculations of nuclear cratering for DNA have been reviewed in detail [16,17]. All are unsuitable for use in defining near-crater environment because of very small predicted craters or other reasons, as summarized in the following graph.

- Nuclear benchmark cratering calculation now in progress at CRT will provide near-crater environment for subsequent phases of this project. It is based on a carefully executed source calculation and uses material models for the Middle Gust III site which have been extensively calibrated in an HE calculation.

Table 4. Summary of Prior DNA Nuclear Crater Calculations

Investigator	Designation	Source	Calc. V/W (ft^3/ton)	Comments[16,17]
Ialango, et al[18]	Large Burst	5 Mt - Source "3"	0.8	Very coarse resolution of final crater (3 cells across rad.). Excessive bulking?
Orphal, et al[19]	ELK 76	same	3.2	Selection of Euler-Lagrange interface probably influence results.
Orphal, et al[20]	ELK 76-DEG.	same	10	Excessive bulking.
Bjork, Kreyenhagen[21]	Big A	1 Mt - Source "0"	84	EOS error.
Ullrich, Dzwilewski[22]	KOA	1.4 Mt "pill"	250	Very coarse resolution of source (3 cells) as simple pill. Unrealistic weakening of lightly shocked material leads to crater formation essentially in a fluid. Material beneath crater still moving downward at 200-300 fps at end of solution.
Cherry, et al	S^3	1 Mt - Source "3/5" over trench	35	Crater predictions made by ballistic extrapolation at 1.2 sec. Crater was still expanding at 20-30 m/sec.

4.3 Numerical Calculation of Middle Gust III HE Crater

- Performed under Contract DNA001-80-C-0265
- Detailed calculation and data comparisons to calibrate materials models and codes for nuclear benchmark crater calculation.
- Provides:
  - stress histories (direct and airblast-induced)
  - displacement histories
- Shows strong influence of interface on motions in typical multi-layered geologies.
- Has recently been extended to 700 msec.

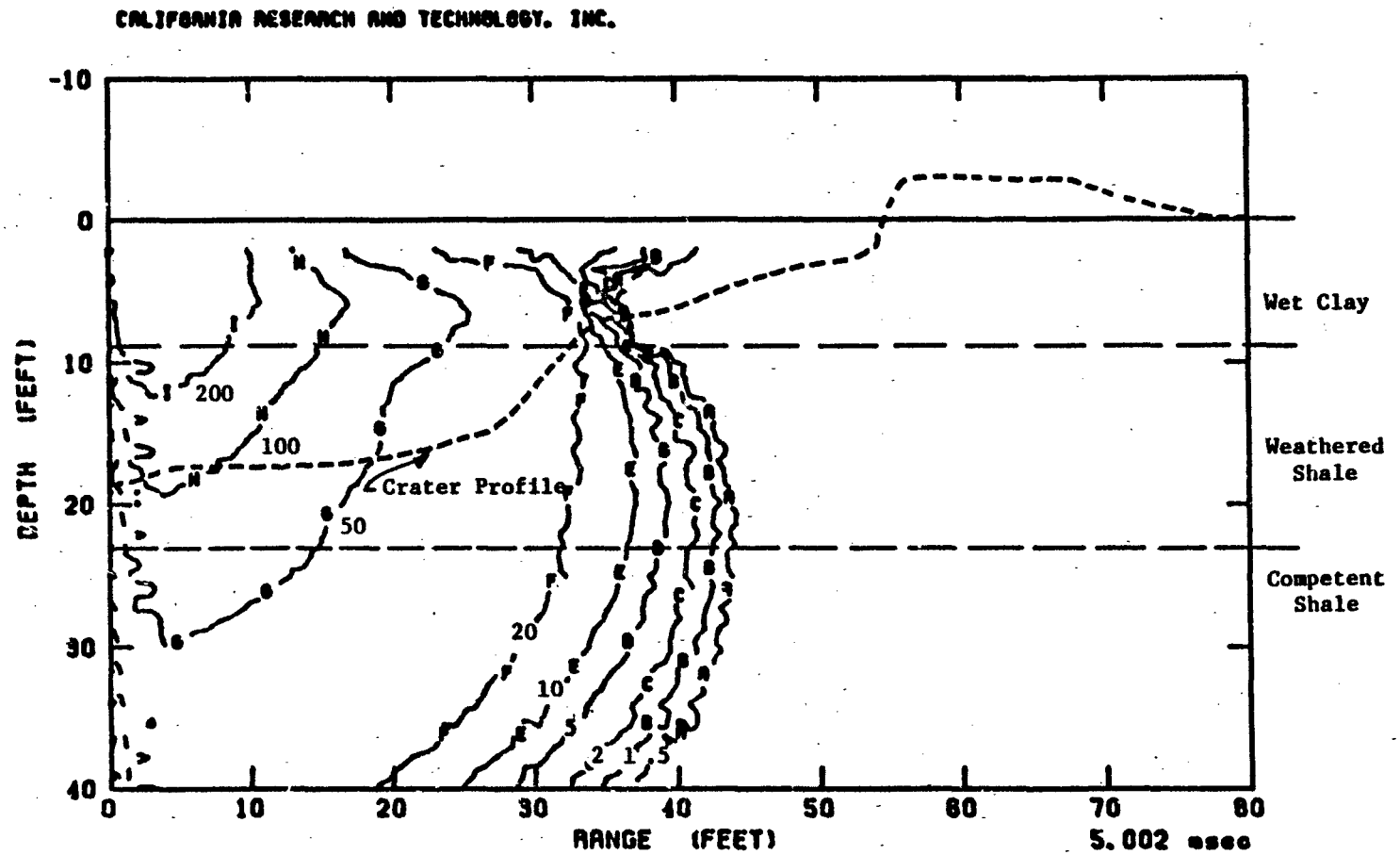

Figure 12. Peak Compressive Stress Contours (in ksi) by 5 msec from Middle Gust III Numerical Simulation.

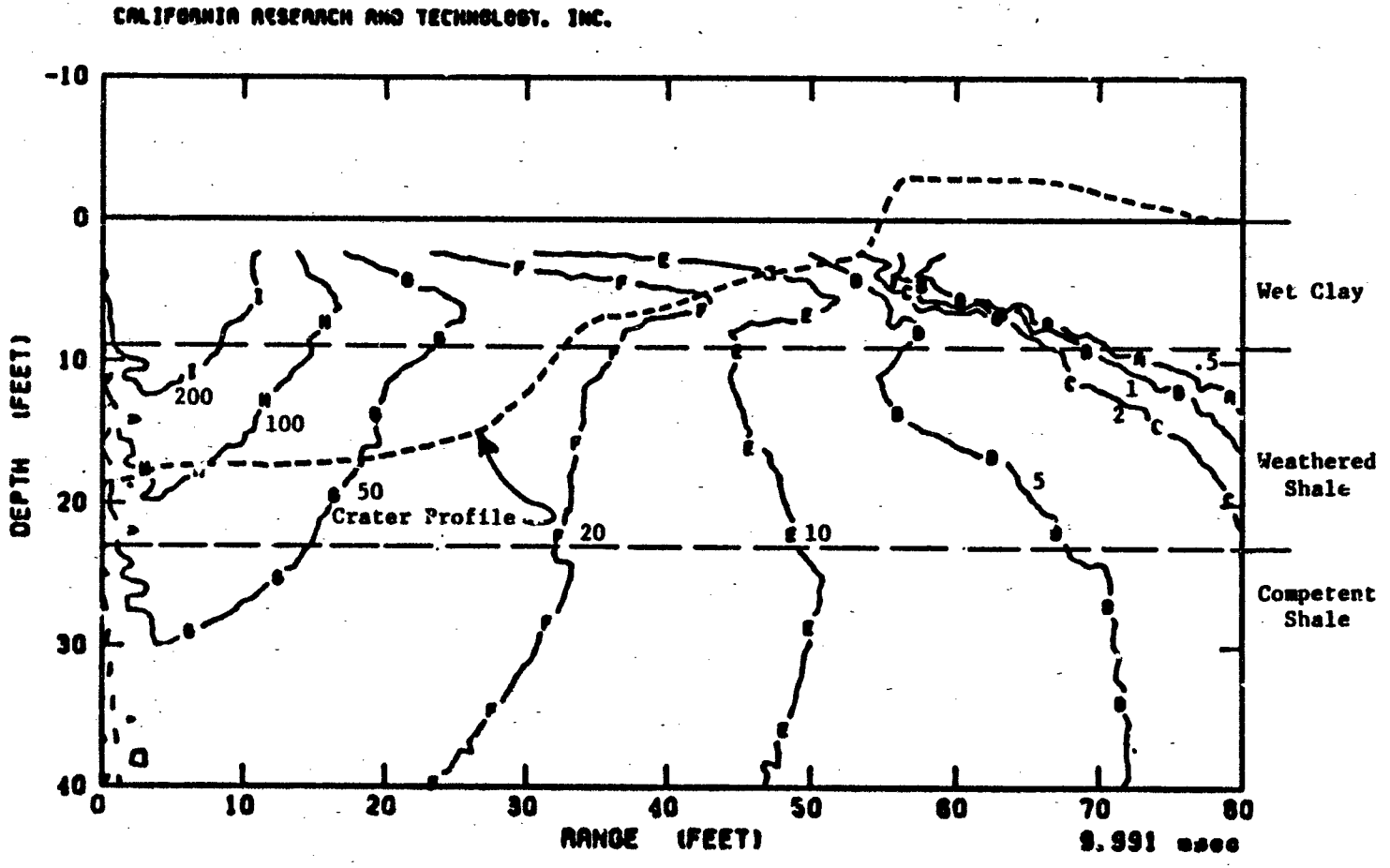

Figure 13. Peak Compressive Stress Contours (in ksi) by 10 msec from Middle Gust III Numerical Simulation.

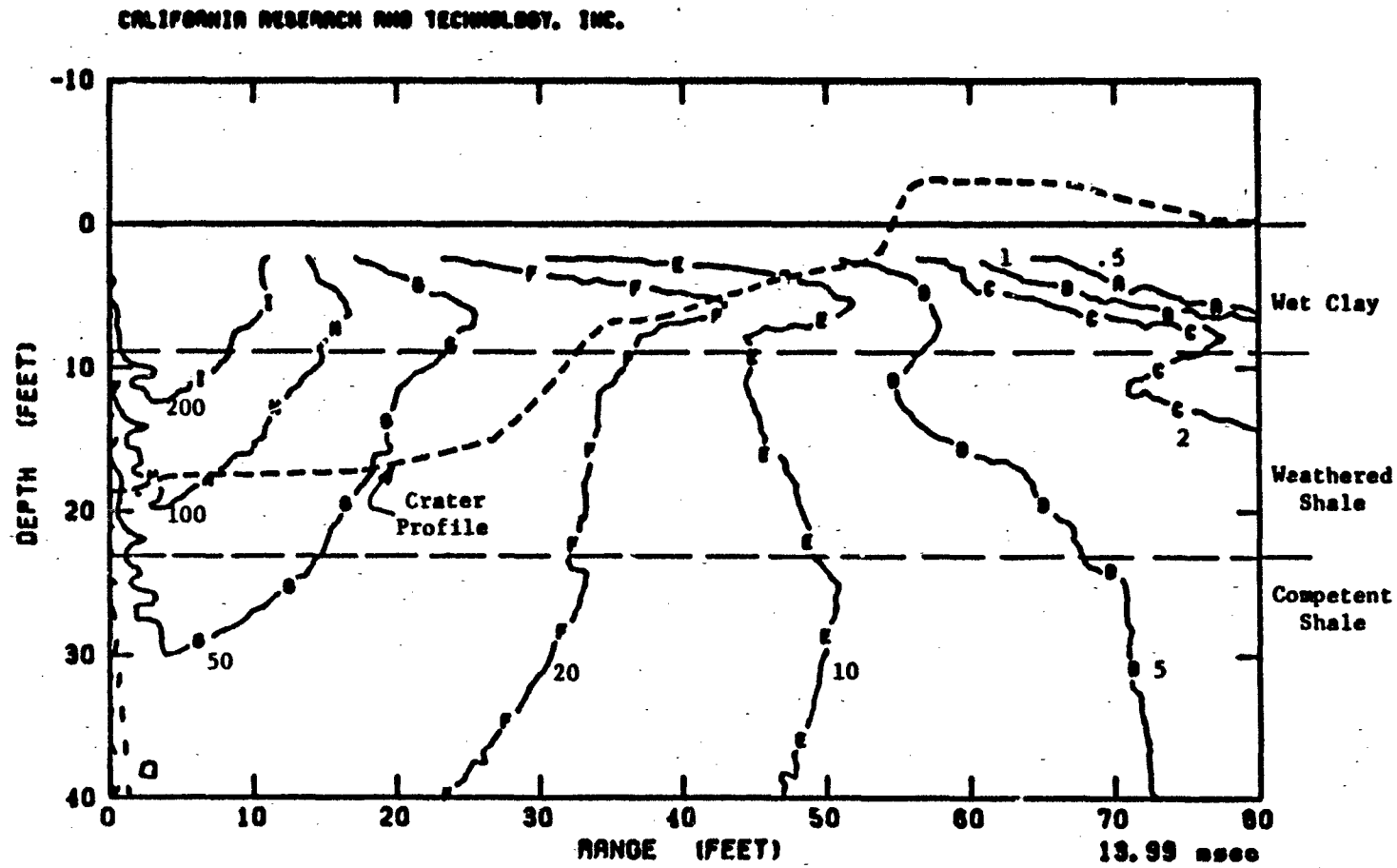

Figure 14. Peak Compressive Stress Contours (in ksi) by 14 msec from Middle Gust III Numerical Solution.

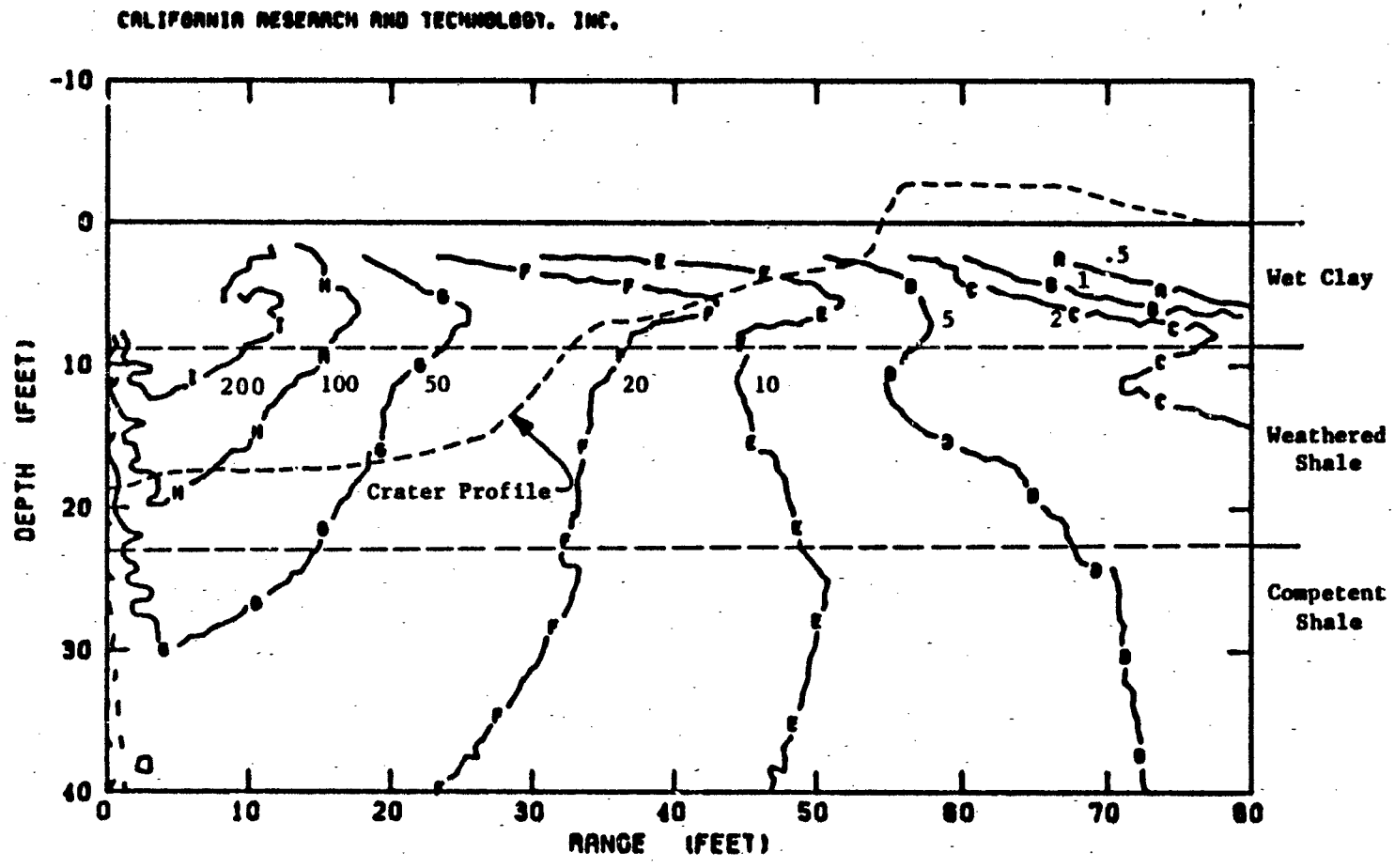

Figure 15. Peak Compressive Stress Contours (in ksi) from Middle Gust III Numerical Simulation. (Note that contours are essentially unchanged after 14 msec).

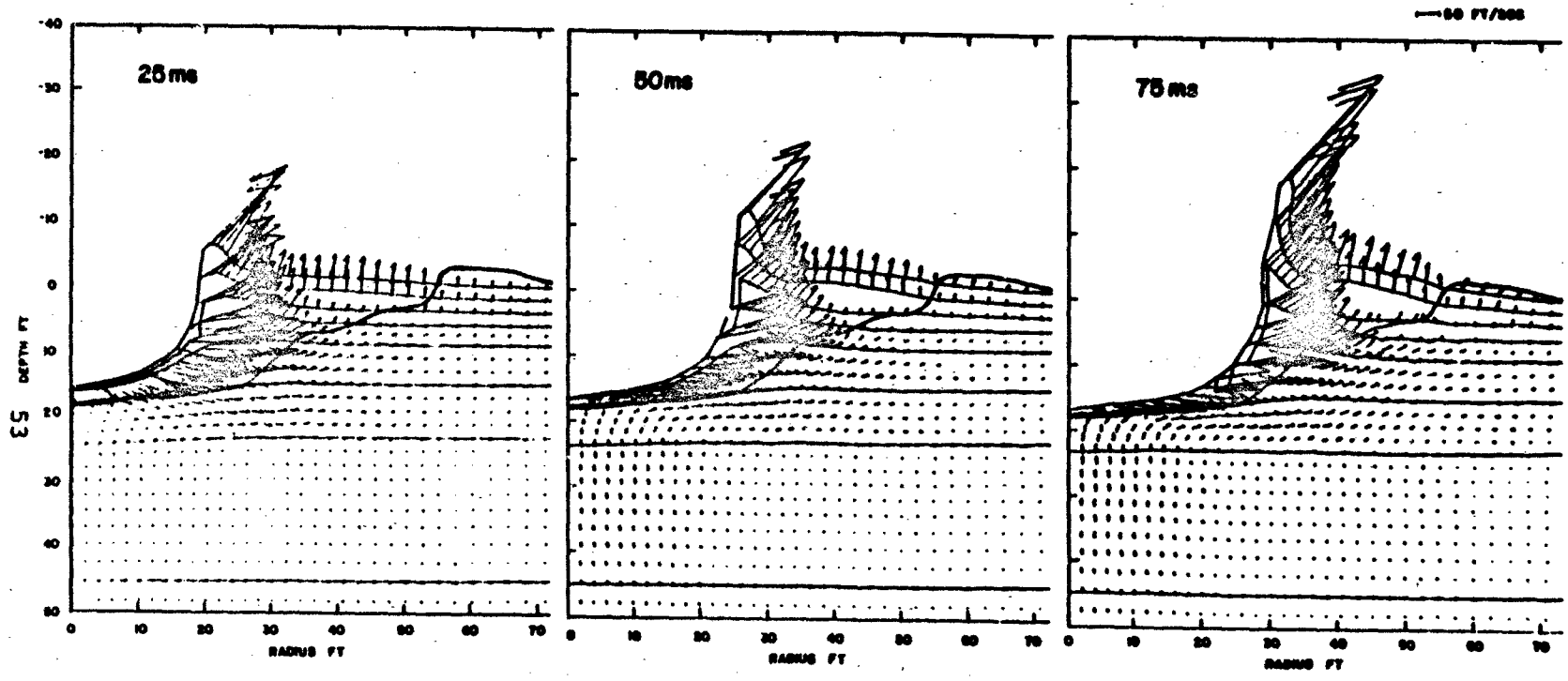

Figure 16. Numerical Simulation of Intermediate-Time Crater Formation of Middle Gust III Event. (Layered geology and crater profile are indicated by solid lines.)

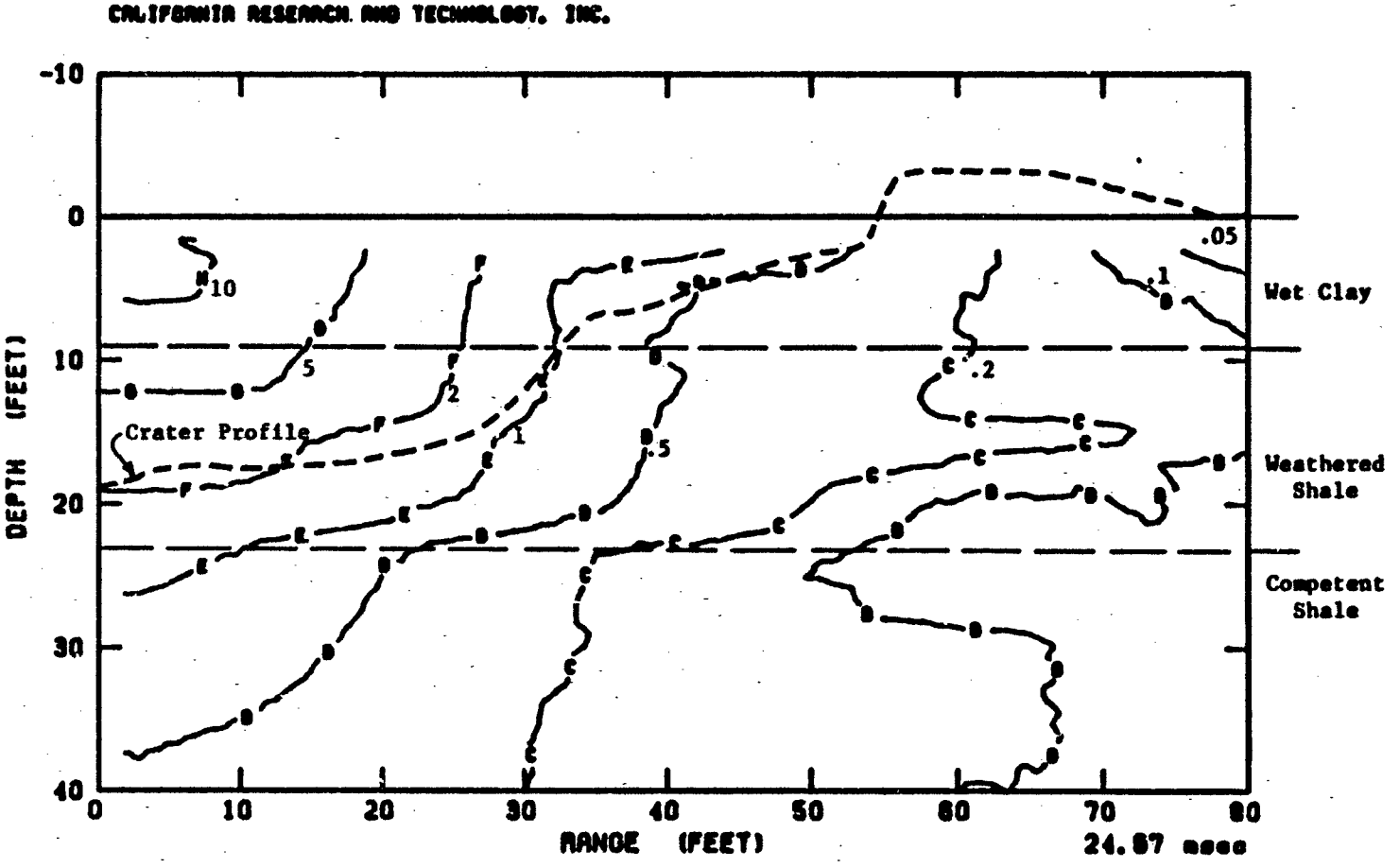

Figure 17. Displacement Controus (in feet) at 25 msec from [illegible]le Gust III Numerical Simulaton.

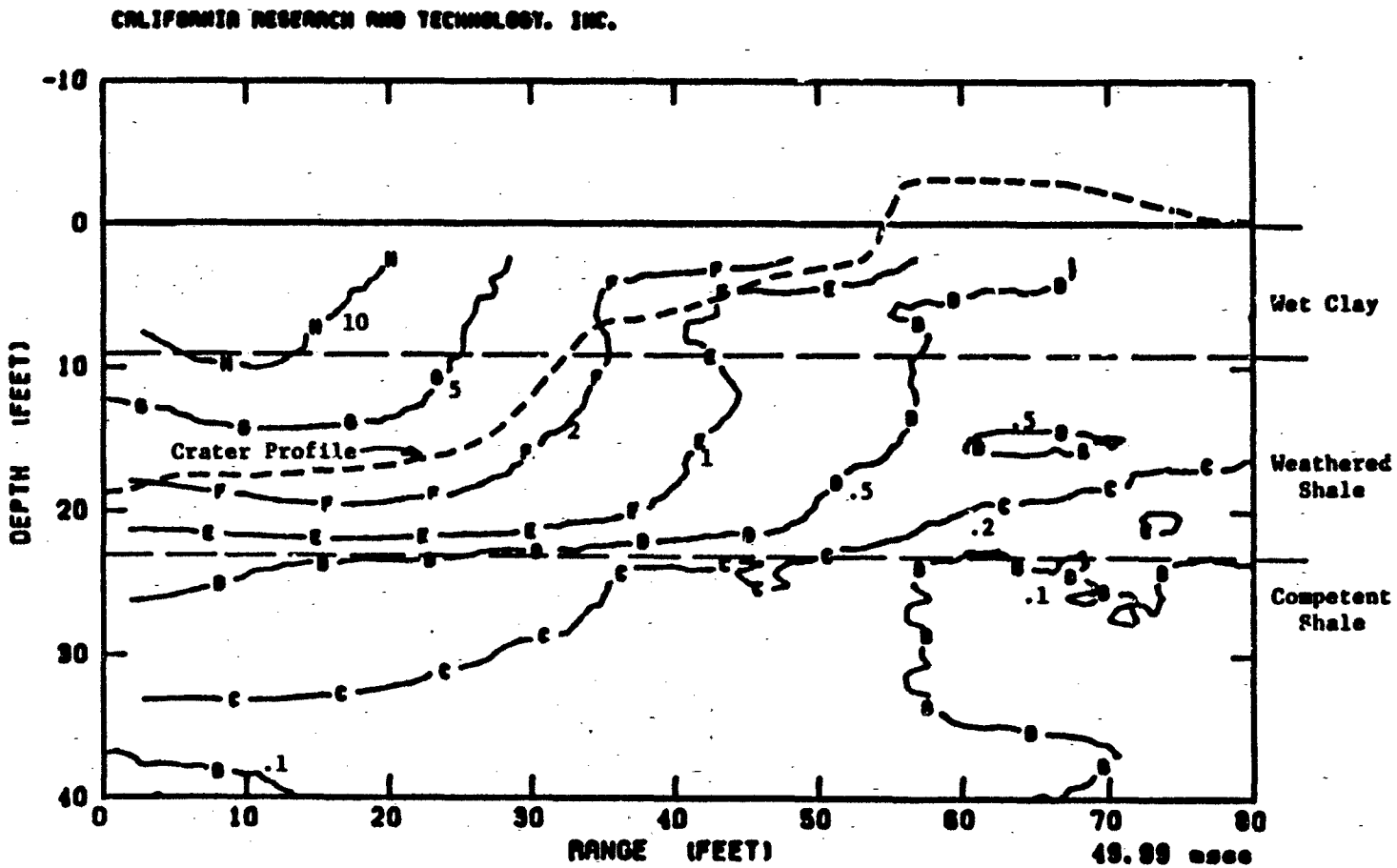

Figure 18. Displacement Contours (in feet) at 50 msec from Middle Gust III Numerical Simulation.

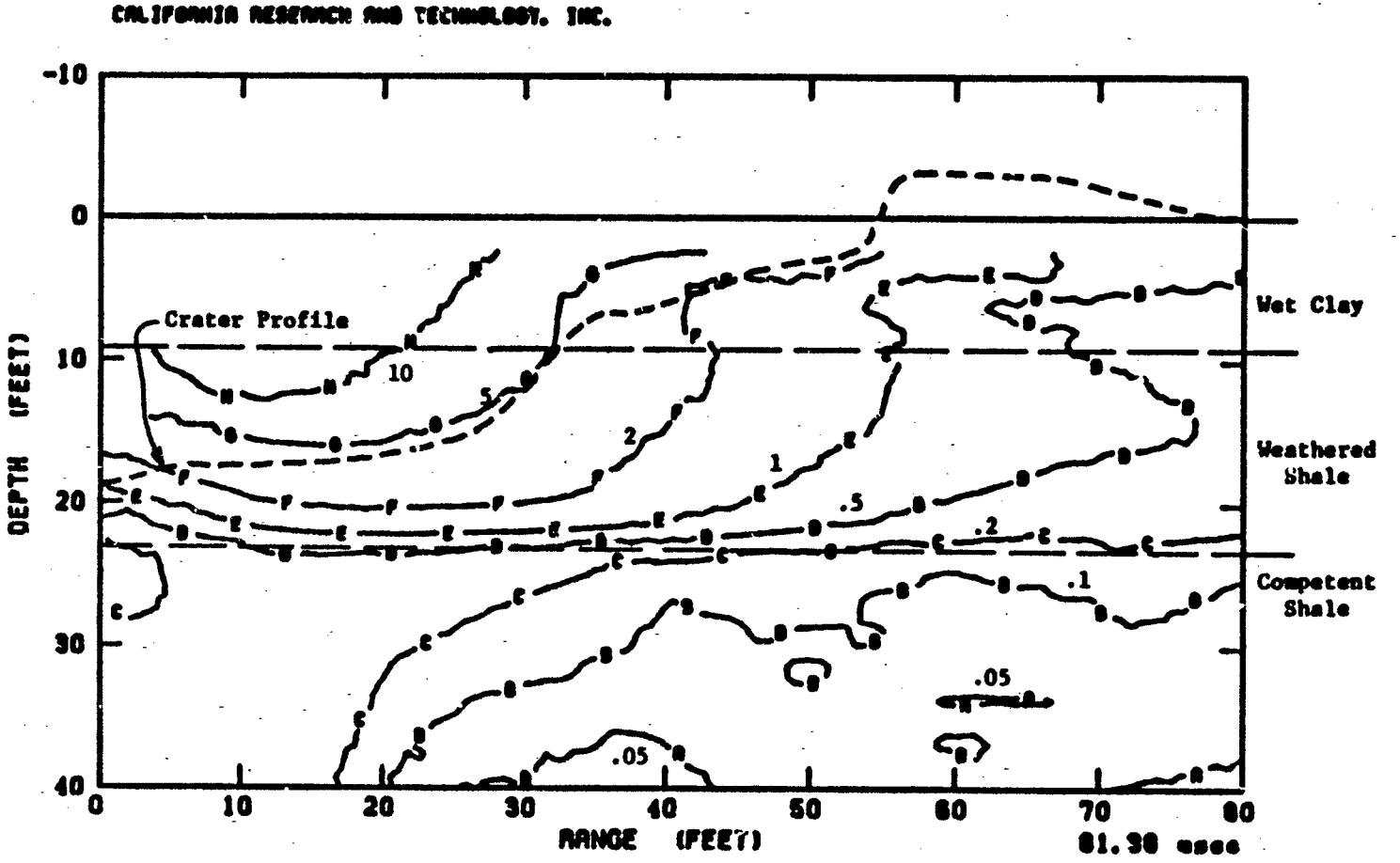

Figure 19. Displacement Contours (in feet) at 80 msec from Middle Gust III Numerical Simulation.

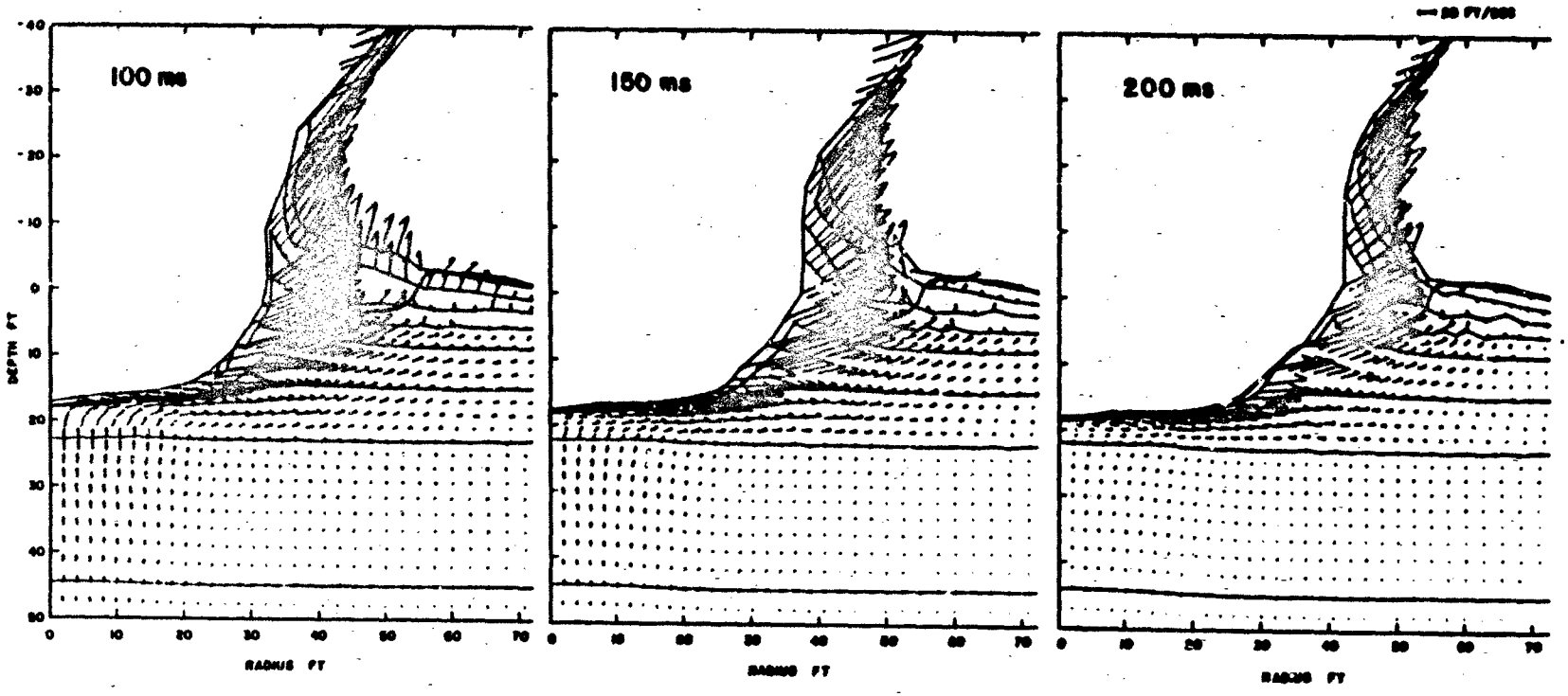

Figure 20. Numerical Simulation of Late-Time Crater Formation of Middle Gust III Event. (Layered geology and crater profile are indicated by solid lines.)

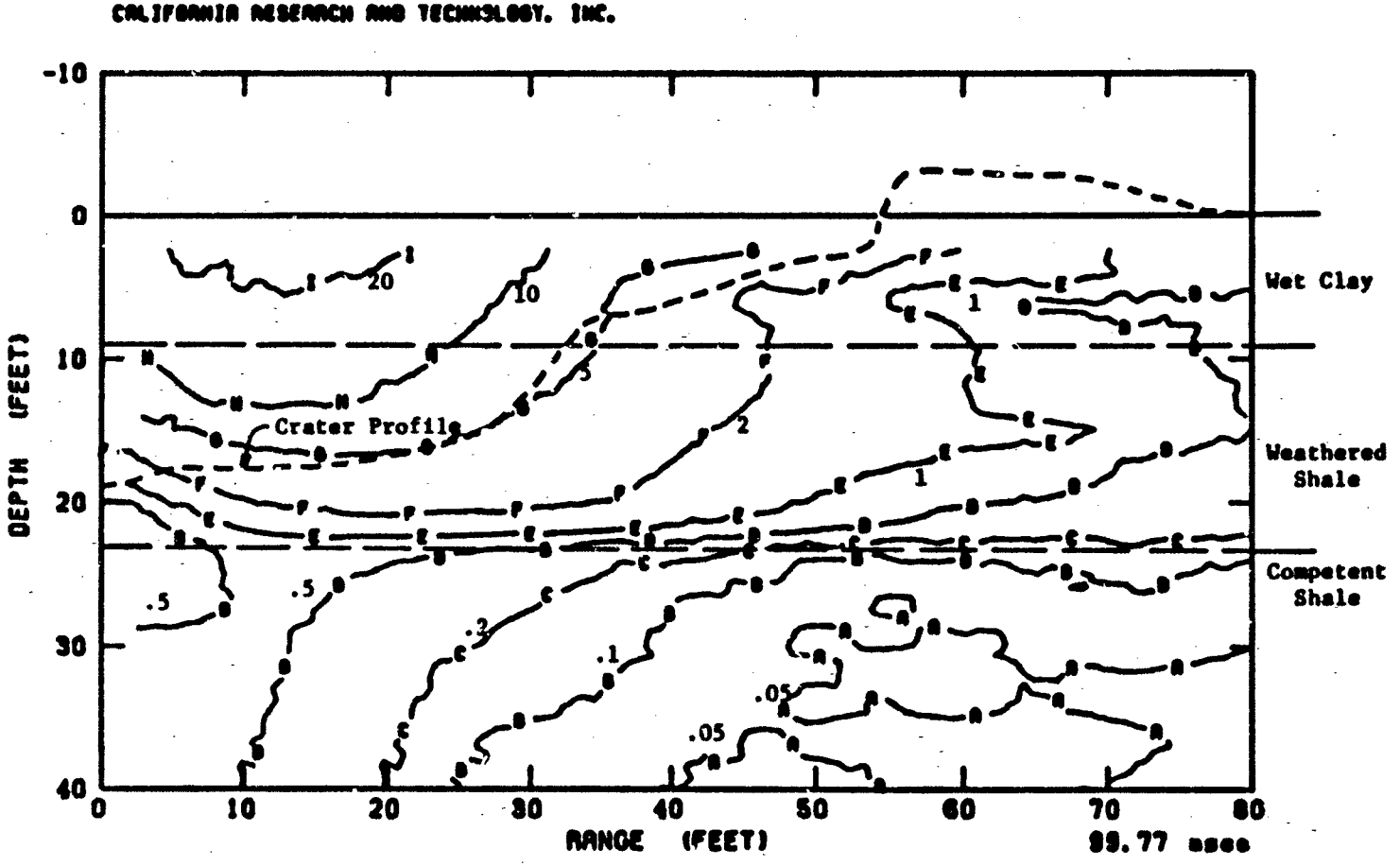

Figure 21. Displacement Contours (in feet) at 100 msec from Middle Gust III Numerical Simulation.

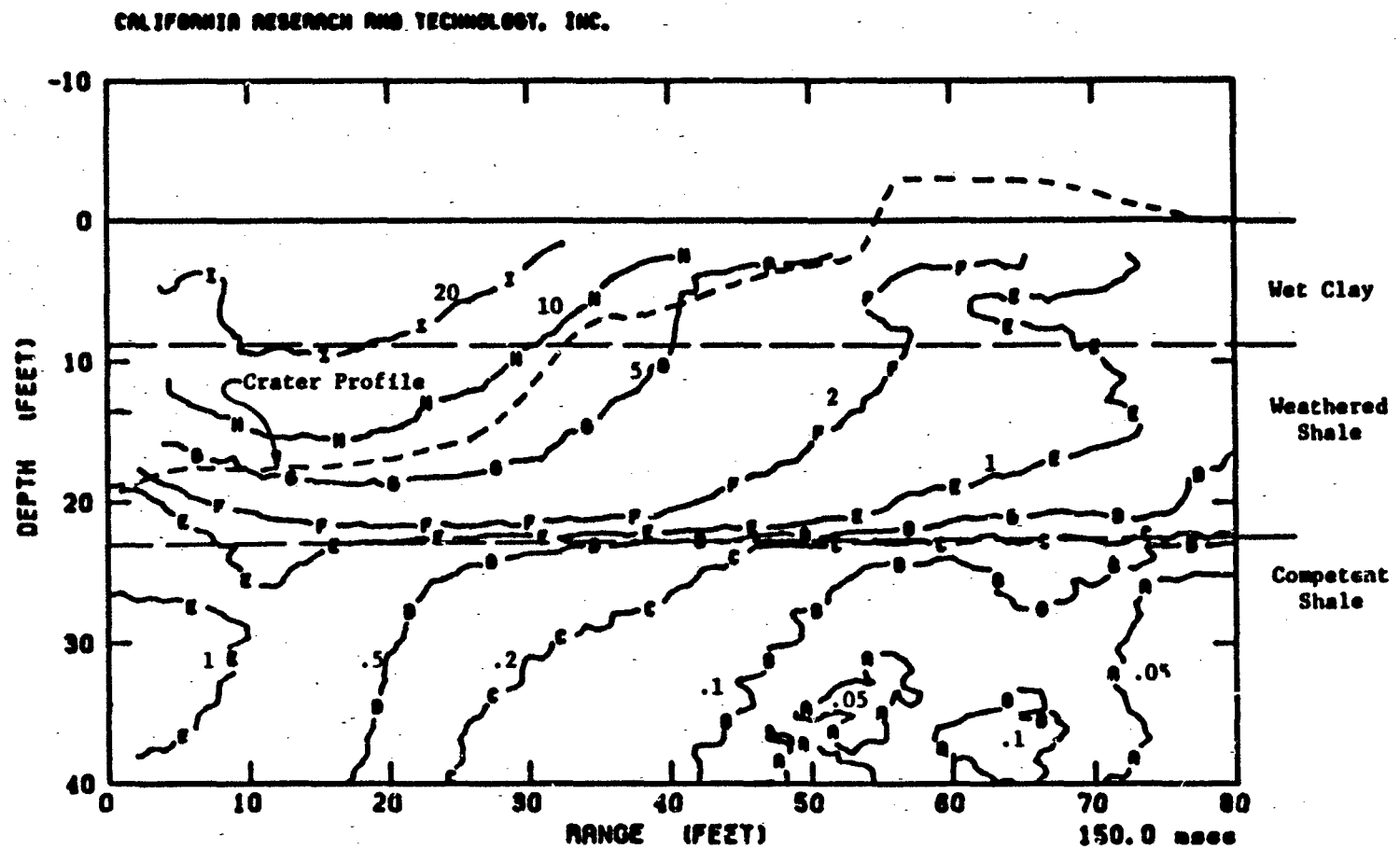

Figure 22. Displacement Contours (in feet) at 150 msec from Middle Gust III Numerical Simulation.

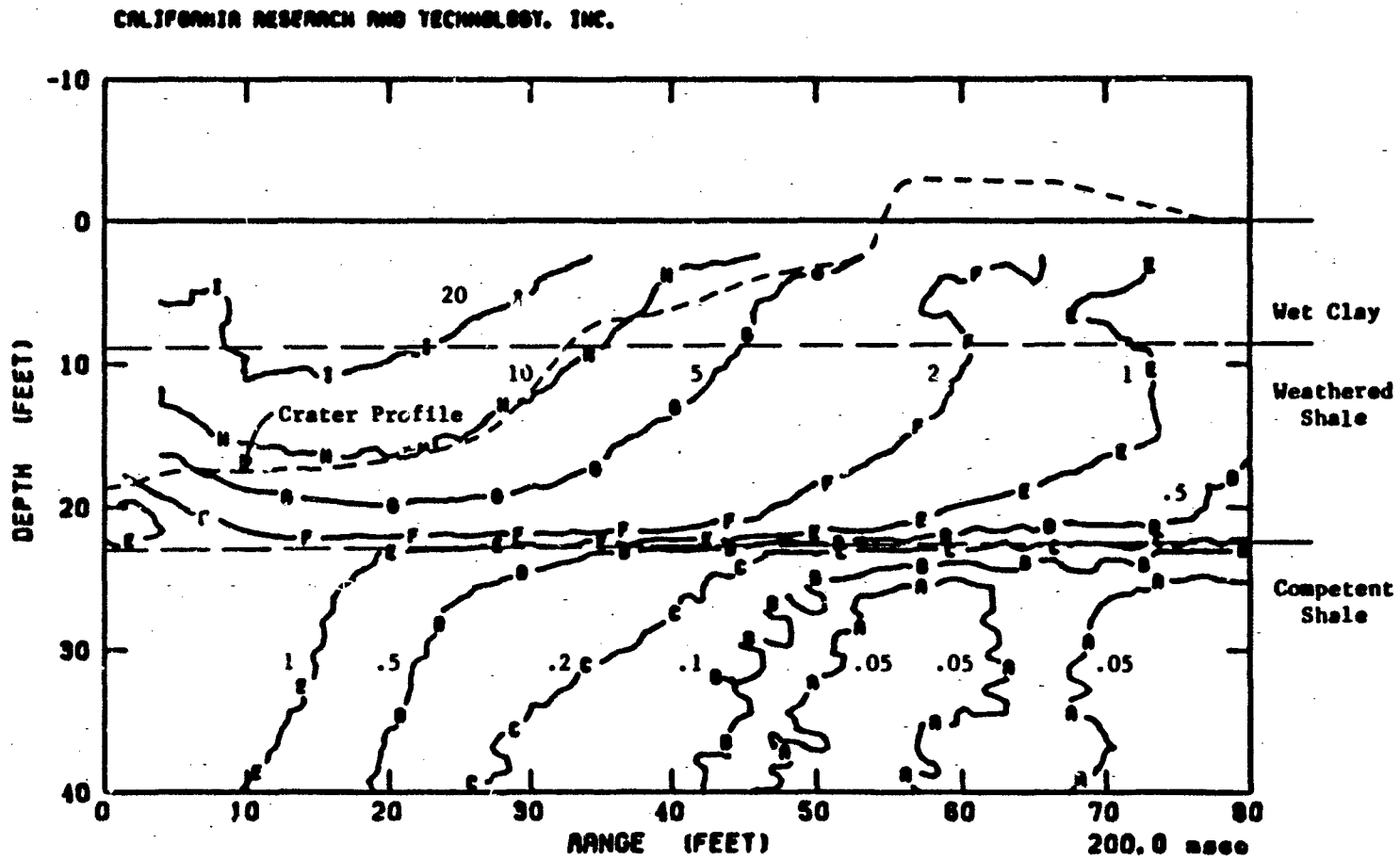

Figure 23. Displacement Contours (in feet) at 200 msec from Middle Gust III Numerical Simulation.

SECTION 5

RESPONSE AND VULNERABILITY OF STRUCTURES NEAR CRATERS

Simplified soil/structure interaction methods have been developed to evaluate the response of structures in the near-crater environment. These techniques are used to examine the separate effects of peak ground shock, dynamic ground shock gradient and cratering flow displacement. Current vulnerability analyses involve the MIDDLE GUST III HE environment as defined by recently completed numerical simulation.

Failure due to Peak Ground Shock:

A finite-element soil/structure analysis was used to evaluate the relationship between free-field stress and soil/structure interface stress. Given this relationship, static collapse analysis was used to determine structural vulnerability due to ground shock.

In the MIDDLE GUST III near-surface wet geology, the peak interface stress was found to be essentially the same as the peak free-field stress. Thus, the predicted collapse contours for typical structural cross-sections are determined using the peak ground shock pressure.

Failure due to Dynamic Ground Shock Gradient:

The early-time bending reponse of structures is excited by the temporal and spatial gradient of the ground shock along the structure length. A finite-element analysis of soil/structure interaction showed that structures are initially accelerated with

the free-field ground shock motion. Thus, the free-field ground shock motion was used to define the early-time dynamic loading on the structure.

Finite-element beam (2-D plane stress) models were used to evaluate the early-time bending response of steel tilt gages, MX-B vertical shelters and STP silos placed in the simulated MIDDLE GUST III dynamic ground shock gradient. The maximum predicted range for destruction of these vertical structures are in the crater margin. It should be noted that the numerical results for the tilt gages are consistent with observed experimental data.

Failure due to Cratering Flow Displacement:

The late-time bending response of structures was evaluated using a quasi-static finite-element beam analysis procedure with non-linear soil springs to account for the soil/structure interaction loads which occur during cratering flow.

The response of steel tilt gages, MX-B shelters and STP silos was considered for the MIDDLE GUST III geology (wet clay over weathered shale), using the calculated free-field crater flow displacement. These results show a substantial drop in peak bending stress near the crater edge and the significant effect of the clay/shale interface.

5.1 Failure Due to Peak Ground Shock

Analysis: Static

Model: Plane Strain Cross-Section

Load: Peak Free-Field Stress

Failure: Collapse Stress

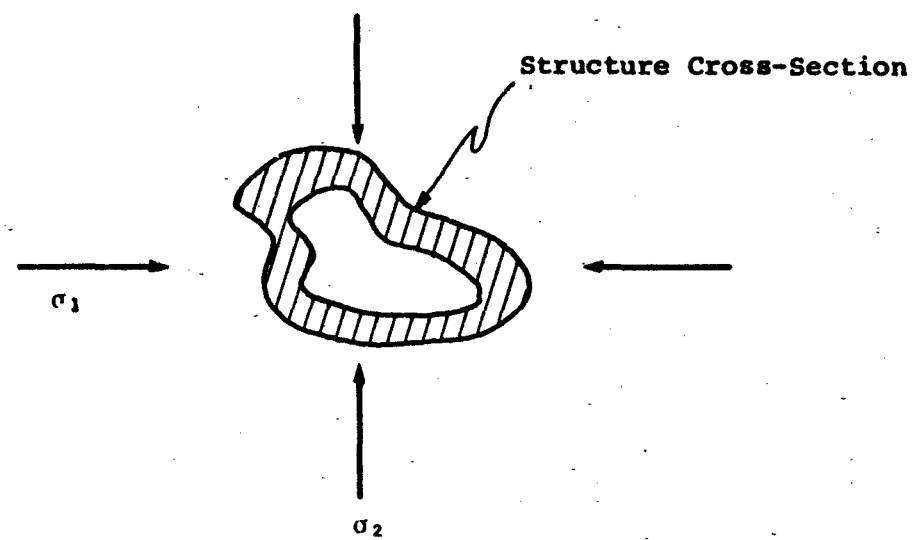

Figure 24. Failure Due to Peak Ground Shock.

- This figure illustrates the numerical procedure used to evaluate the loading of buried thin wall sections due to ground shock. The procedure uses the free field ground shock pressure histories given by finite difference cratering analysis as boundary conditions to a soil island containing the soil/structure interface and structure.

- With this modeling approach, a relation between the free field ground shock pressures and the soil/structure interface pressures can be determined for various geologies, and generic structures. This soil/structure island approach accounts for increases in soil/structure interface pressures associated with dynamic wave reflection and also can account for soil/structure interface pressure reduction associated with soil arching. Both these effects are highly problem dependent and their influence on structural response can be significant.

- The soil/structure island approach was considered necessary in order to evaluate appropriate relationships between free field soil pressures and soil/structure interface pressures. Given this relationship, uncoupled simplified analyses can then be employed to evaluate structural failure.

Evaluation of Structural Loading of Thin-Walled Structures by Ground Shock

1. From finite difference cratering analysis, define free field ground shock around soil island containing structure location.

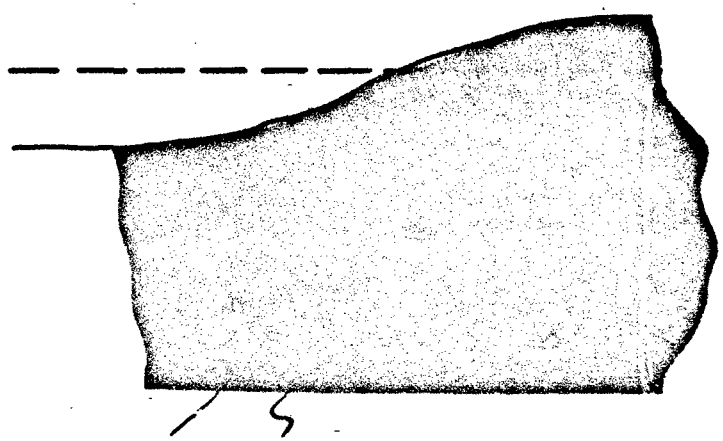

2. Use free field ground shock pressure histories as boundary conditions on soil/structure finite element model to determine soil/structure interface pressures.

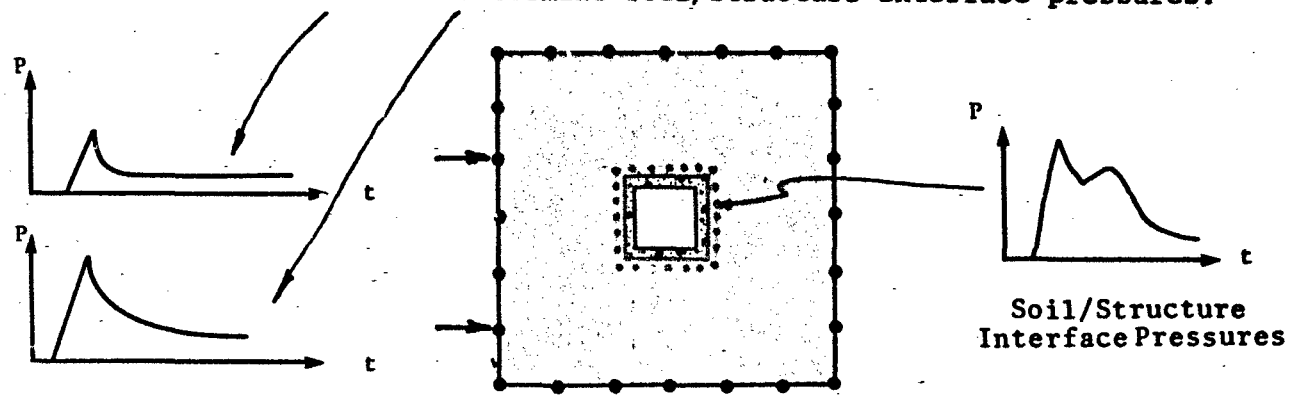

Figure 25. Evaluation of Structural Loading of Thin-Walled Structures by Ground Shock.

- This figure shows the plane strain soil/structure island model used to evaluate the loading of a concrete box structure (t/ℓ = .125) located near the surface (5 ft depth) and placed at various ranges in the Middle Gust III environment.

- The intent of the soil/structure island model is to determine appropriate magnification or reduction factors for free field versus soil/structure interface pressures typical of structures placed in Middle Gust wet clay soils and shale.

Finite Element Soil/Structure Island Model Used to Evaluate Interaction with Ground Shock

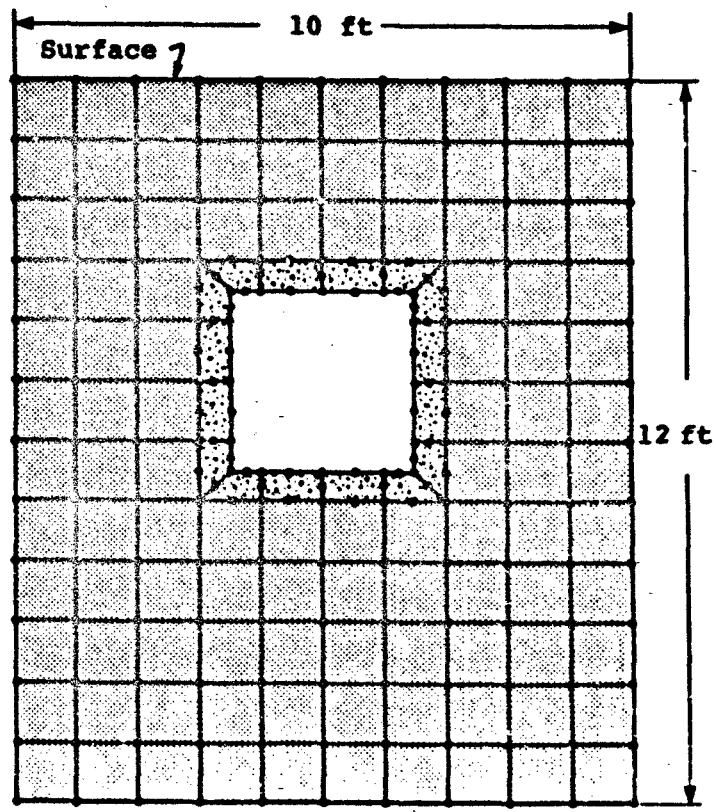

Figure 26. Finite Element Soil/Structure Island Model Used to Evaluate Interaction with Ground Shock.

- This figure gives a comparison of Middle Gust III free field pressures applied to the soil/structure island model with the calculated pressures applied to soil/structure interfaces located in the wet clay. In this medium, the peak soil/structure interface pressures are essentially equivalent to the free field soil pressures. Such behavior is typical of low strength soils, where states of stress remain essentially hydrostatic. Thus, soil arching (reduction in soil/structure interface pressures caused by an increase on the load carried by the soil) is not significant in wet clay under these conditions. This is consistent with experimental data from Kiger [23].

- For the Middle Gust III environment in the wet clay layers, soil/structure interface pressures associated with ground shock are shown to be essentially equivalent to the free field pressures. Thus, structural analyses for collapse can be performed based on static analyses using peak free field pressures.

- For structures in shale, or in media like sand, where shear strength increases with pressure, soil arching plays a significant role in structural collapse, as shown by Kiger [23,24]. For these geologies, analysis based on peak free field soil pressures would not be applicable.

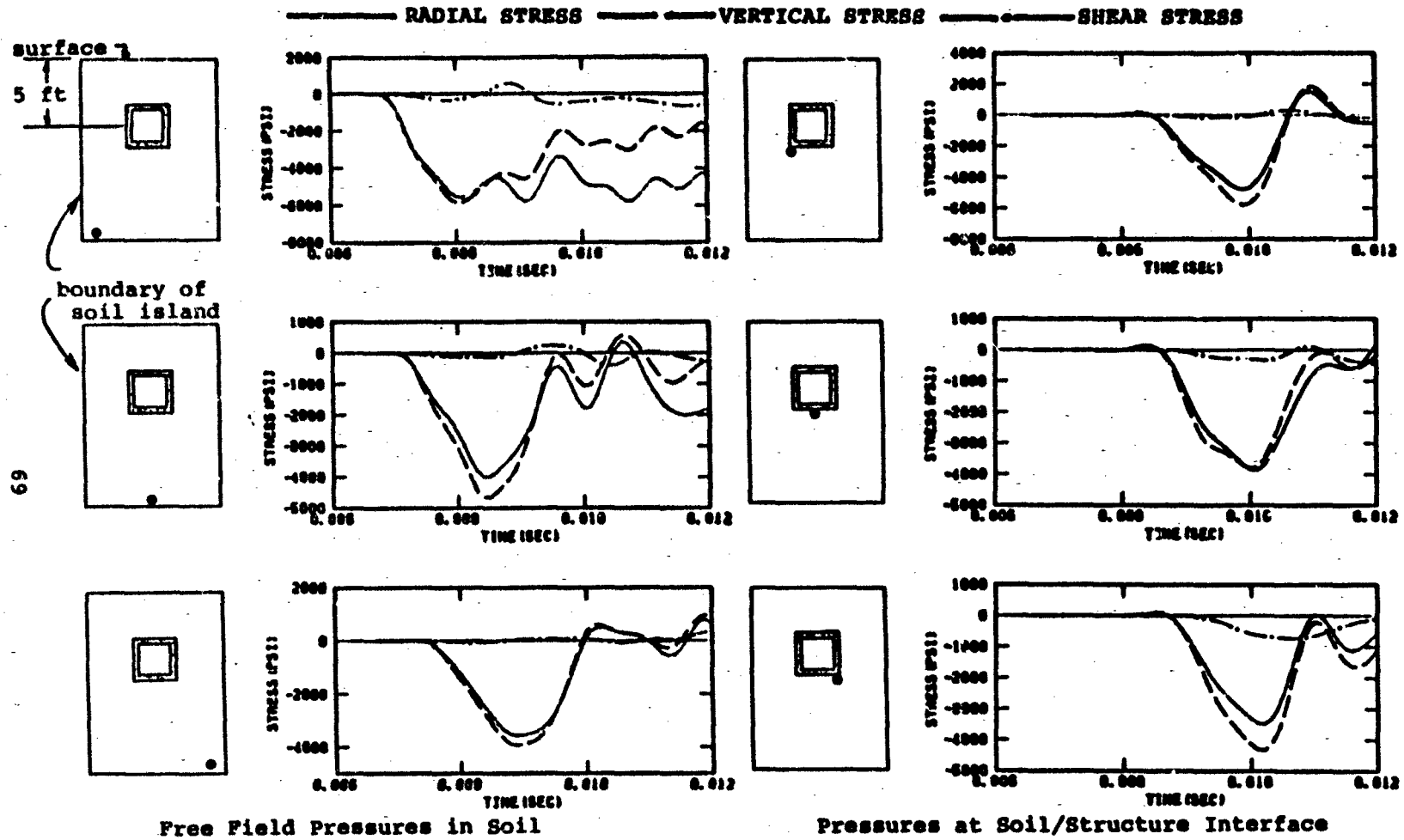

Figure 27. Comparison of Free Field Soil Pressures with Pressures on Soil/Structure Interface at 55 ft Range in MIDDLE GUST III Environment.

- Since the free-field pressures were found to be essentially equivalent to the soil/structure interface pressures in the wet clay Middle Gust III geology, static analyses were used to evaluate collapse of various structures based on the peak ground pressures.

- This figure shows the static collapse pressure for various steel cross-sections.

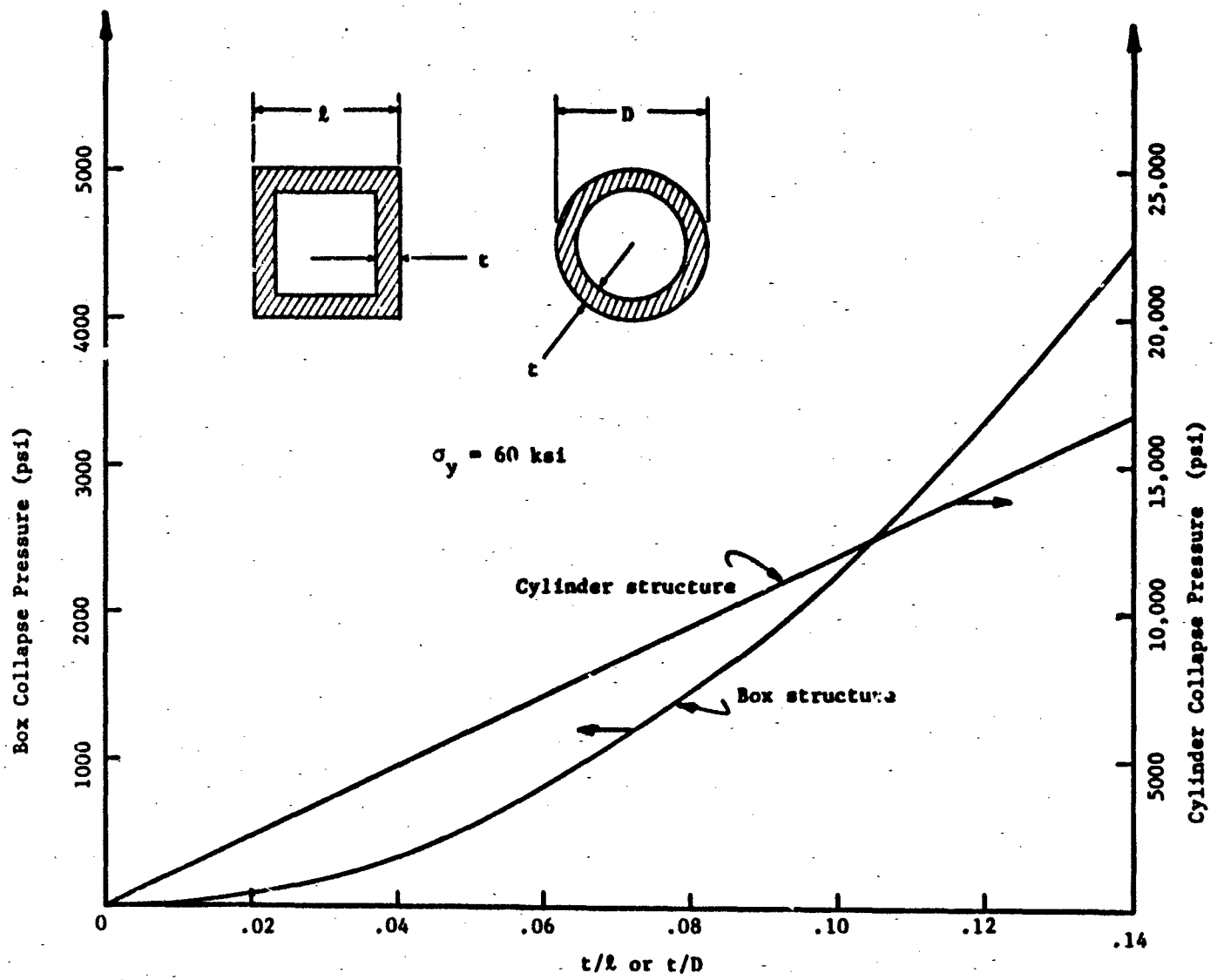

Figure 28. Static Collapse Pressure for Thin-Walled Steel Box and Cylinder Structures

- This figure shows the static collapse pressure for reinforced concrete cross-sections.

- Note that the MX-B shelter (t/d = .12) and the STP silo (t/d = .20) have static collapse pressure of 1200 psi and 2000 psi, respectively.

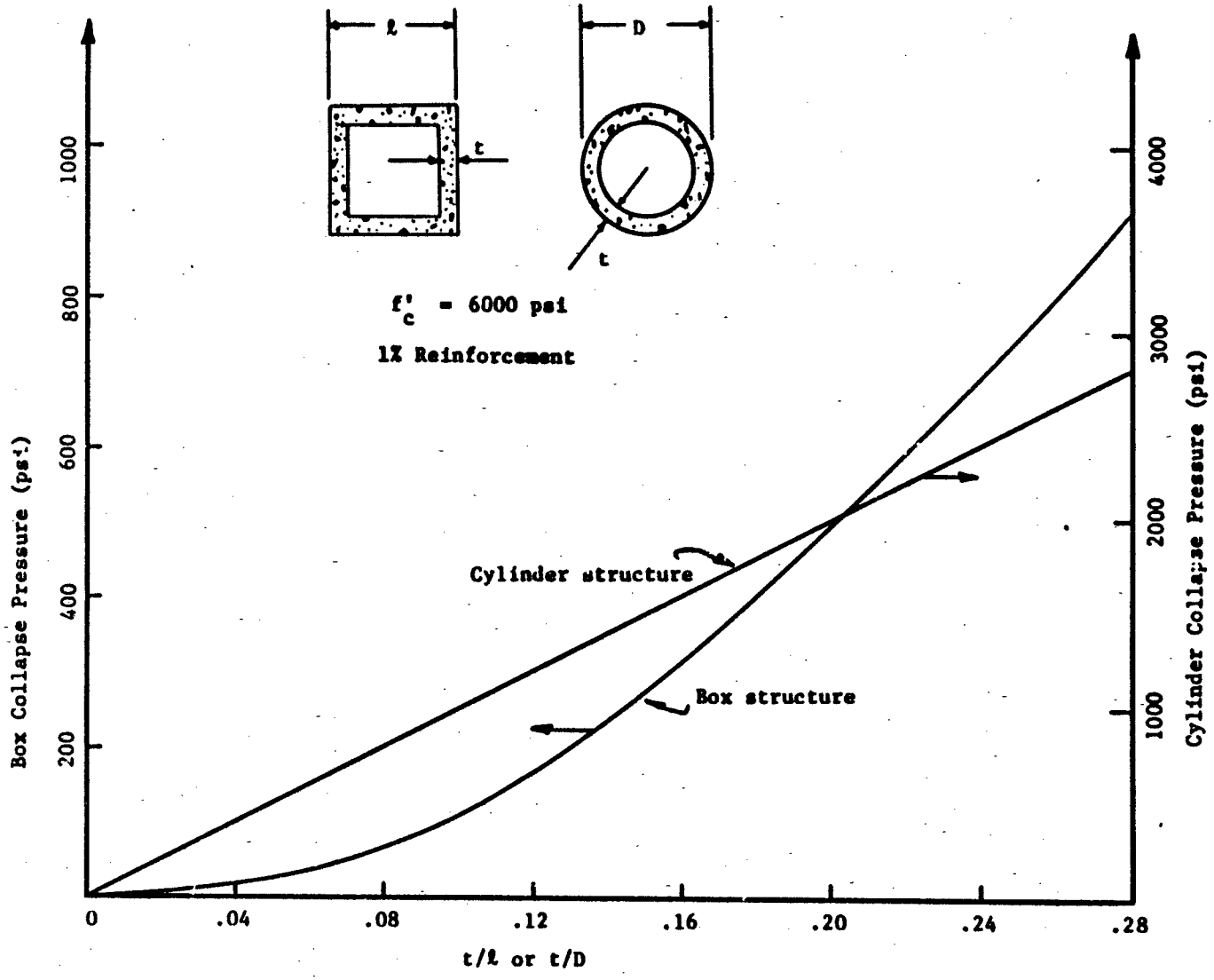

Figure 29. Static Collapse Pressure for Thin-Walled Concrete Box and Cylinder Structures

Based on the static collapse analysis for Middle Gust III peak ground shock:

- Collapse contours for reinforced concrete box ($t/\ell = 0.28$) and cylinder ($t/d = 0.12$) extend out from near the crater edge.

- Collapse contours for steel box ($t/\ell = 0.14$) and cylinder ($t/d = 0.08$) are shallow in the crater to near its edge.

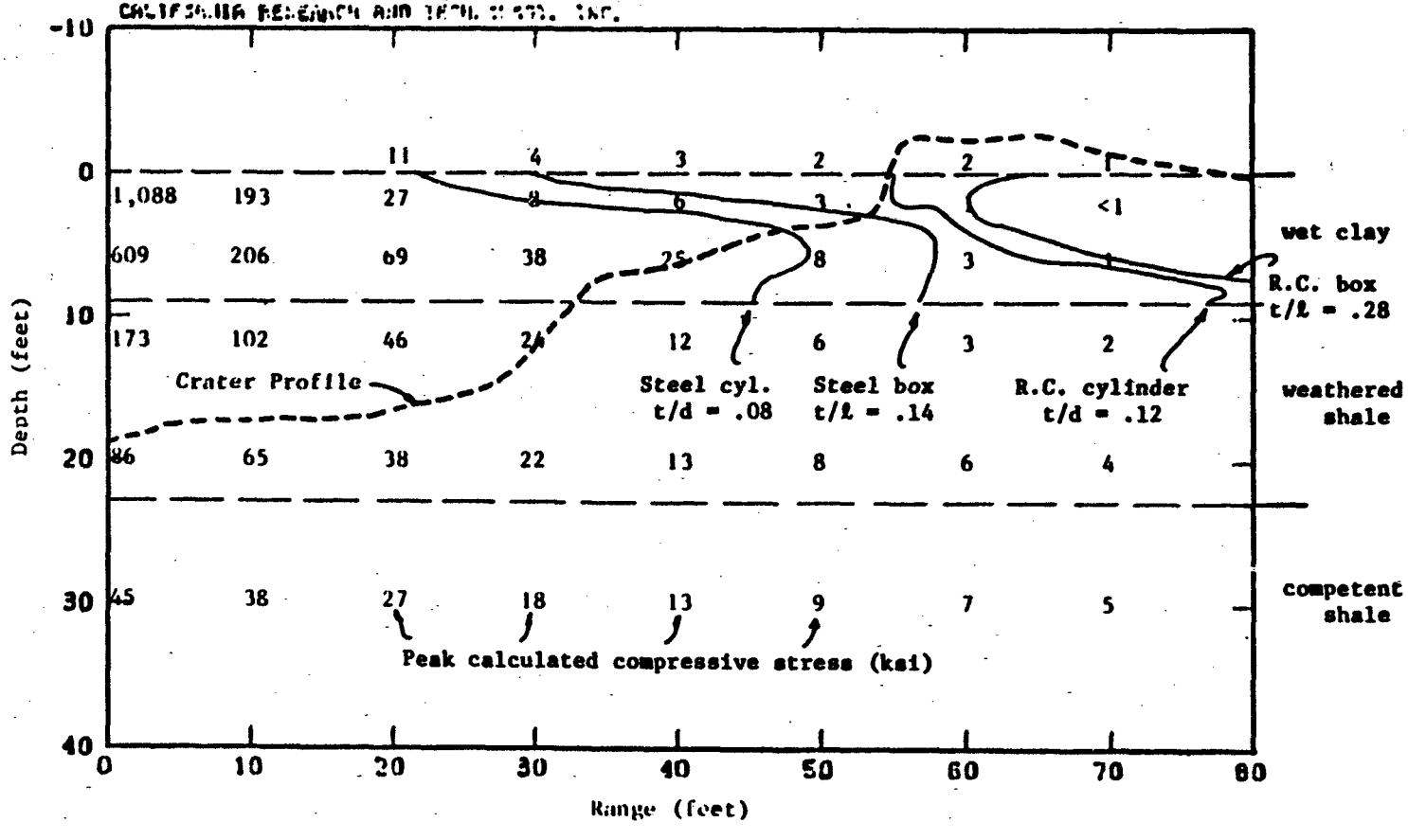

Figure 30. Predicted Collapse Contours for Structural Cross-Sections in MIDDLE GUST III Wet Clay Layer, Based on Peak Compressive Stress.

5.2 Failure Due to Dynamic Ground Shock Gradient

Analysis: Dynamic

Model: Beam Structure

Load: Forces based on idealized fits to early velocity-time histories

Failure: Plastic Hinge

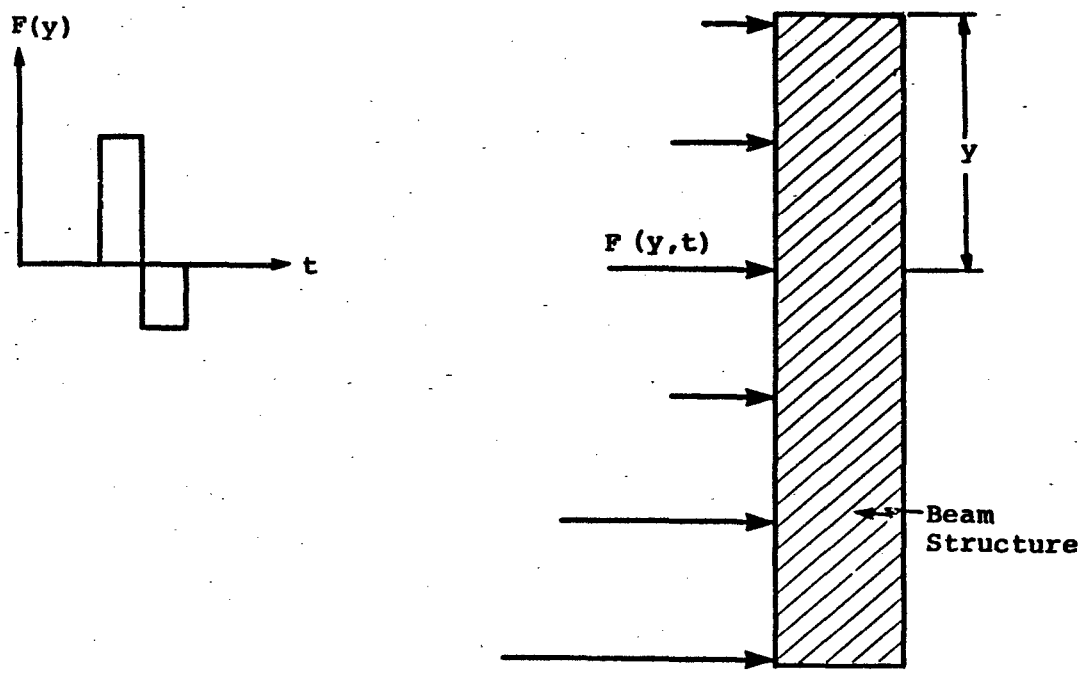

Figure 31. Failure Due to Dynamic Ground Shock Gradient.

- The bending response of buried beam-type structures is excited by the arrival time and spatial gradient of the ground shock motion along the length of the structure.

- In this analytical procedure the free field ground shock motion is used to define the dynamic loading on a finite element beam model of the structure.

- The external loading for the decoupled beam model of the structure is determined by assuming each section of the beam would move with the prescribed motion of the free field provided no shear transfer occurred across stations of the beam.

Evaluation of Structural Bending Response Due to Ground Shock Gradient

1. From finite difference cratering analysis, define the free field ground shock motions at range of structure. Note that shock amplitude and arrival time vary with depth along structure.

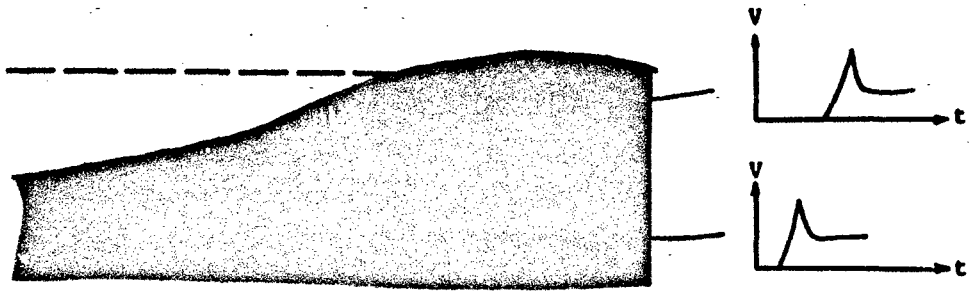

2. Evaluate structural response associated with ground shock gradient, using a decoupled beam model. Beam impulse loading is determined assuming that each section of the beam moves with the free field soil during shock engulfment.

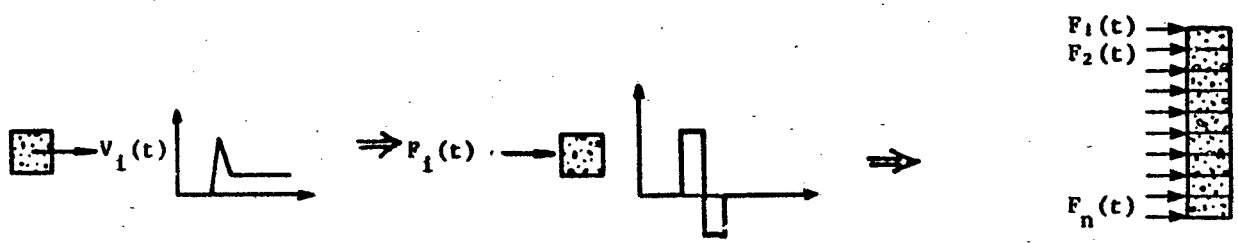

Figure 32. Evaluation of Structural Bending Response Due to Ground Shock Gradient.

- This figure illustrates a typical beam model (2-D plane stress) of a 6-inch diameter thick-walled steel pipe structure used to evaluate the early time bending response of tilt and rotation structures placed at various ranges in Middle Gust III. Three different length structures were tested, 5', 9' and 20'. These were placed near the surface starting at the 40 foot range. A post-test examination of thest structures indicates that all structures placed outside the crater edge (i.e., > 50 foot range) did not experience severe inelastic response. However, some of the structures placed inside the crater failed. Furthermore, the shorter structures (5' and 9') failed, whereas the 20' length tilt structures remained functional.

- Using the analytical procedures previously mentioned, the various tilt structures placed in Middle Gust III were analyzed to evaluate the effects of ground shock gradient on their bending response. The results of these analyses are summarized in the subsequent plots.

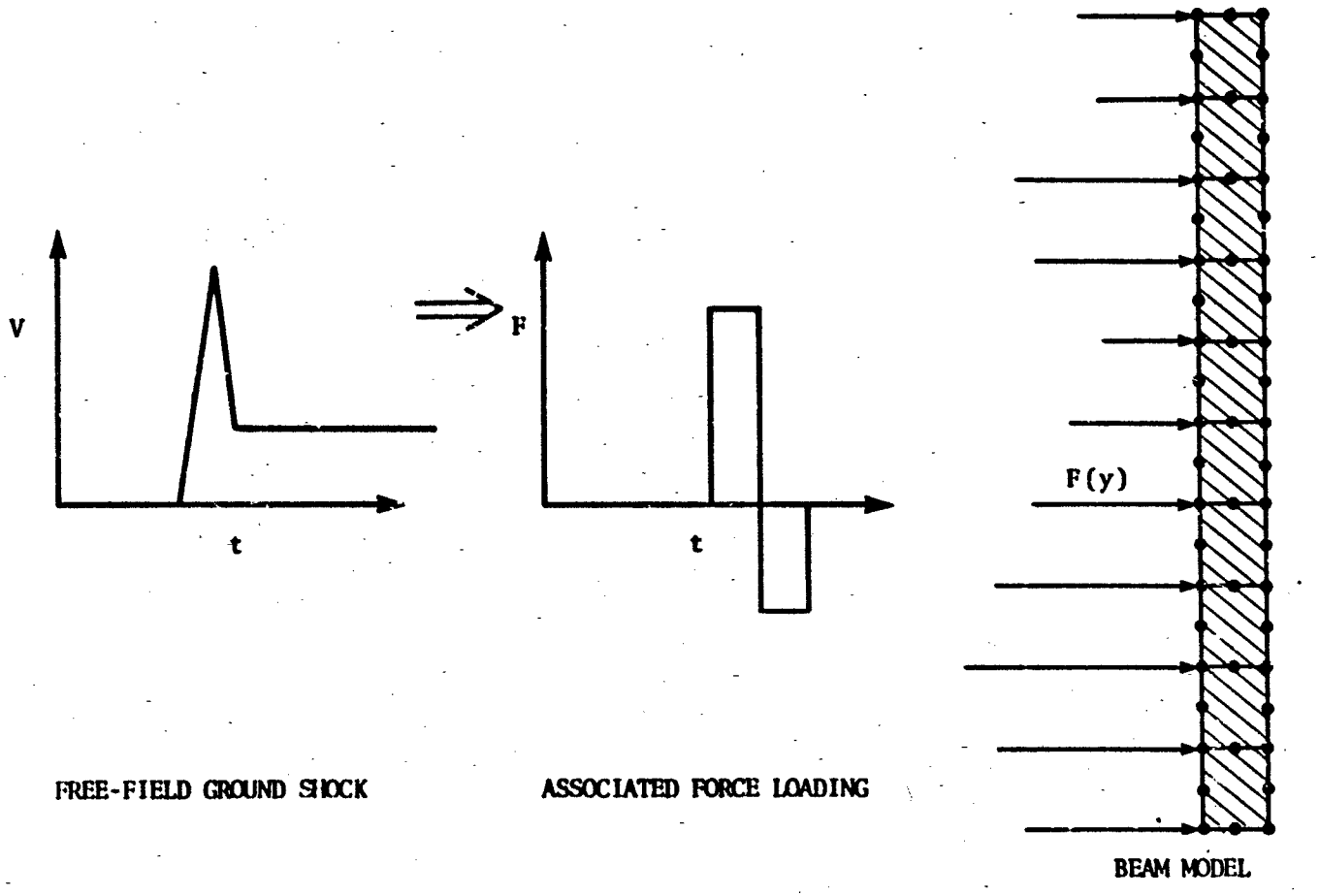

Figure 33. Beam Model of Buried Steel Tilt Structure in MIDDLE GUST III Environment.

- This figure shows the calculated bending stress distribution at times of peak amplitudes in the 5, 9 and 20 foot length tilt structures placed at the 40 foot range. Also given are the periods of the first three fundamental modes of vibration and the time it takes for the ground shock to travel up the length of each structure. From the stress distribution it is observed that the three structures respond differently due to the ground shock loading. That is, the ground shock excites essentially the first mode in the shortest structure, the second mode in the 9-foot structure and the third mode in the longest structure. Essentially because of this difference, peak stress amplitudes in the longest structure are predicted to be smaller than in either of the shorter gage structures. Clearly, the bending response of such vertical beam-type structures to non-simultaneous arrival of non-uniform ground shock loading is highly dependent on arrival times along the structure and the specific response mode which is thereby excited.

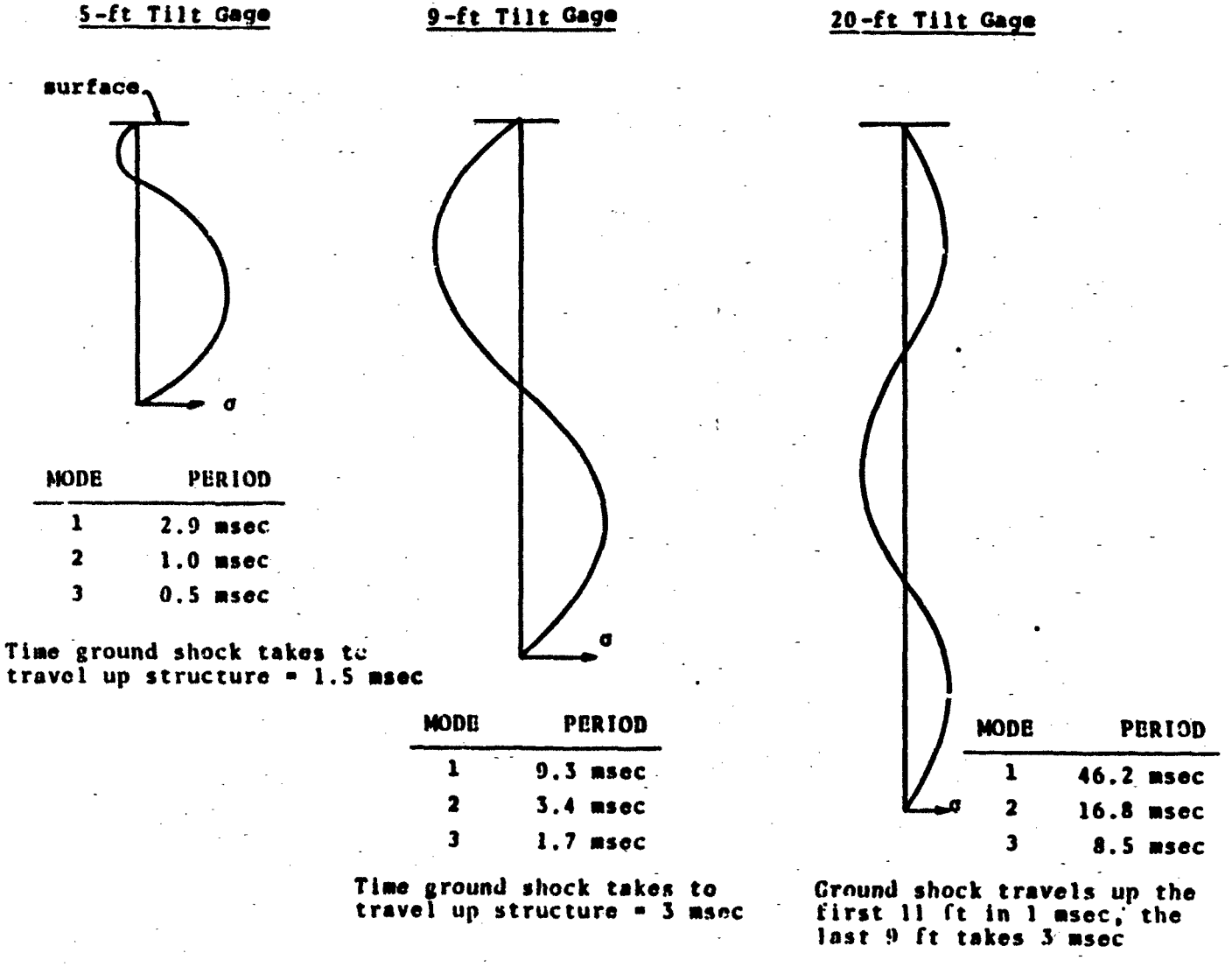

Figure 34. Comparison of the Bending Stress Distribution at Times of Peak Amplitudes in the 5, 9, and 20-ft Tilt Gage Structures at 40-ft Range in MGIII Environment.

- This figure gives the calculated peak bending at various ranges determined for 9' length tilt structure, assuming a 60 ksi material yield stress and a perfectly plastic stress/strain law, the tilt structure can resist an elastically determined bending stress of 90 ksi, whereupon a plastic hinge forms. Based on this failure criterion, failure of the 9' tilt structure caused by the ground shock gradient will occur for structures placed inside the 45 foot range. These numerical results are consistent with observed experimental data.

- These numerical results also indicate that the 5' length structures (125 ksi) are stressed higher than the 9' (110 ksi) and the 20' (75 ksi) structures placed at the 40 foot range. These numerical results are also consistent with experimental test results [10], i.e., at this range, 5' and 9' structures were destroyed whereas 20' structures remained functional.

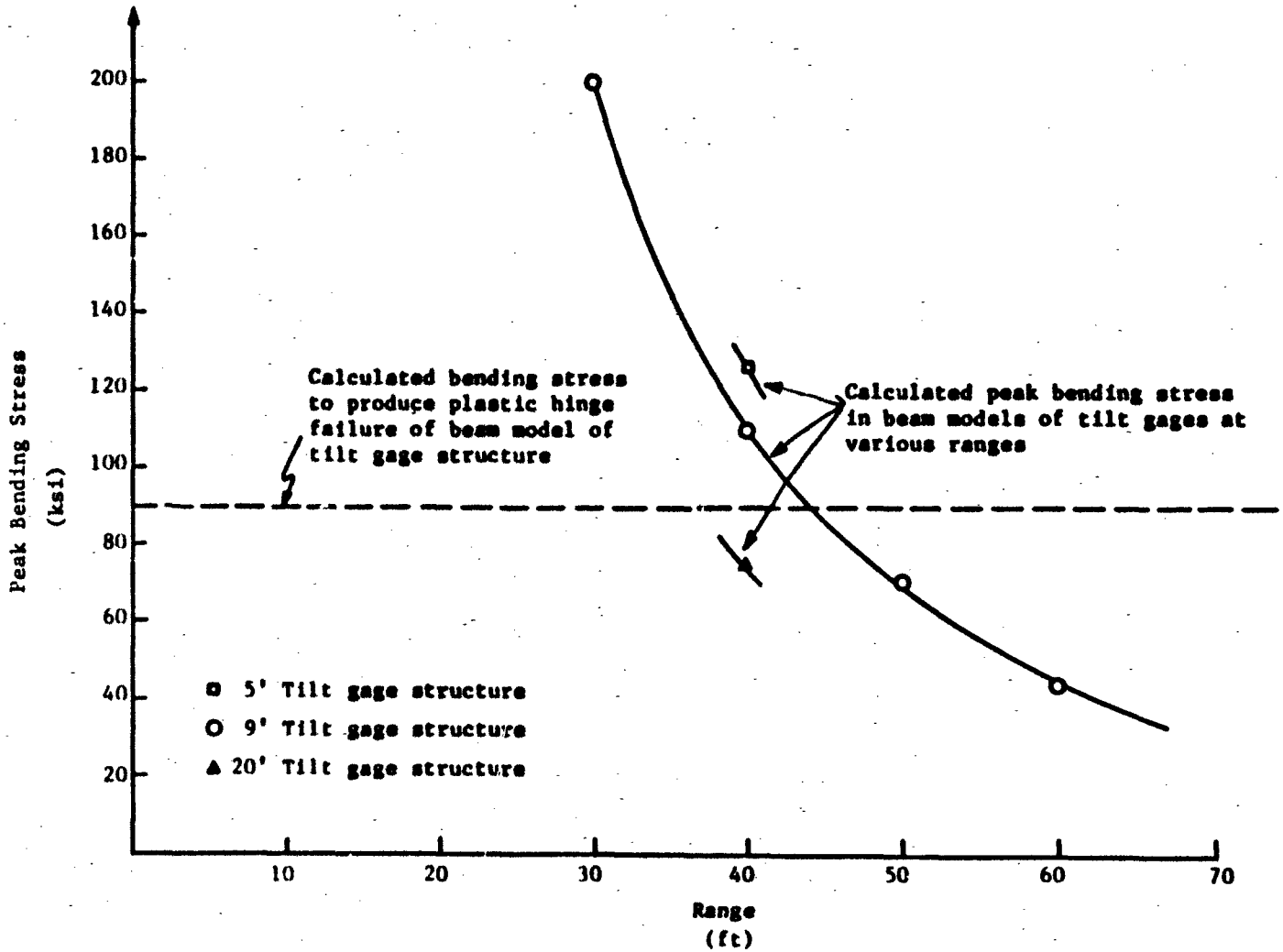

Figure 35. Calculated Peak Bending Stress in Tilt Gage Structures in the MIDDLE GUST III Environment at Various Ranges.

- In a similar manner this plot gives the calculated peak bending stress as a function of range for scaled MX-B vertical shelters and STP silos due to the ground shock gradient of the Middle Gust III environment.

- These structures are predicted to be destroyed within the crater margin.

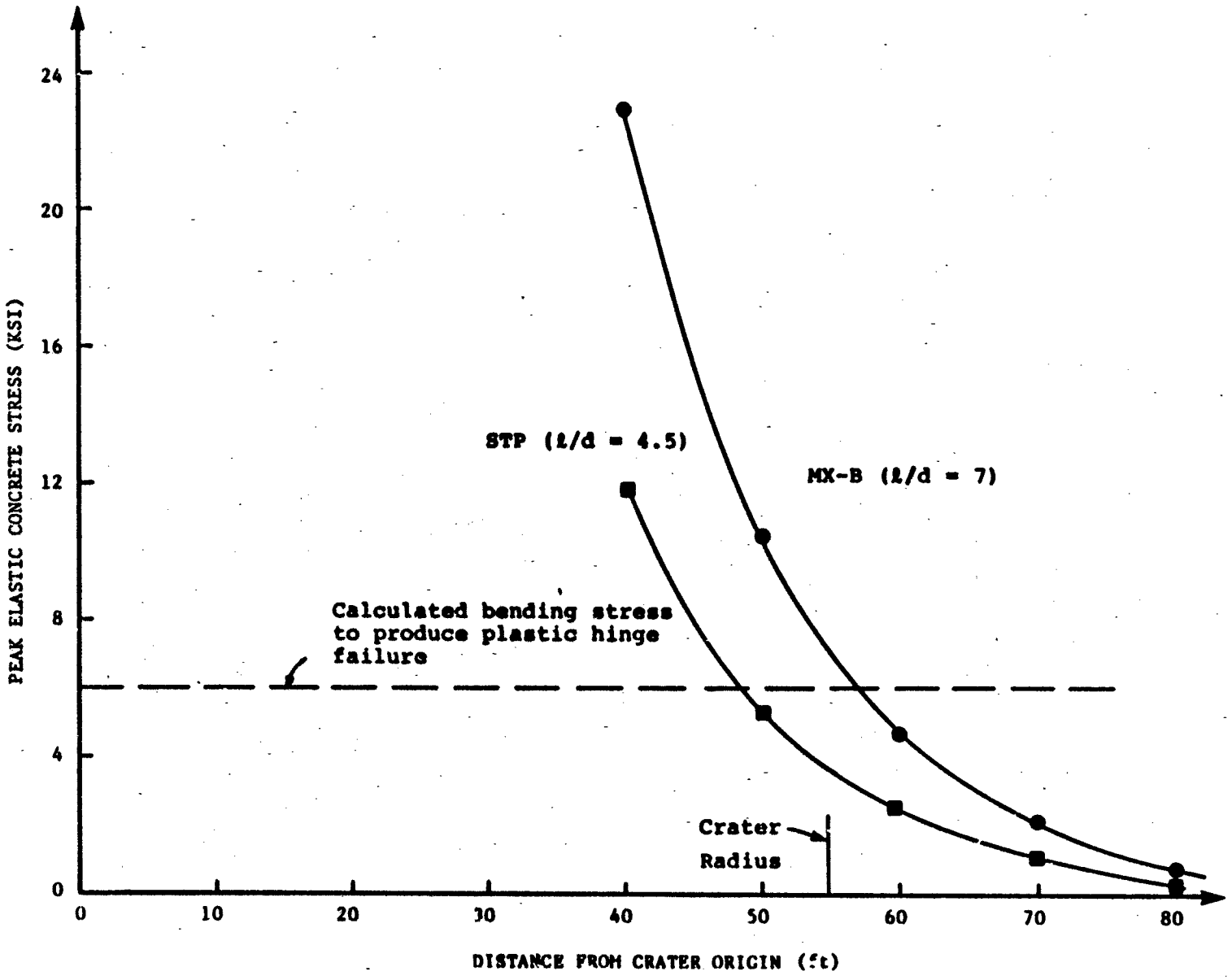

Figure 36. Calculated Peak Bending Stress Due to Ground Shock Gradient in Vertical Structures Placed in MIDDLE GUST III Environment.

- This figure gives the maximum predicted range for destruction of vertical structures due to effects of ground shock gradients in Middle Gust III.

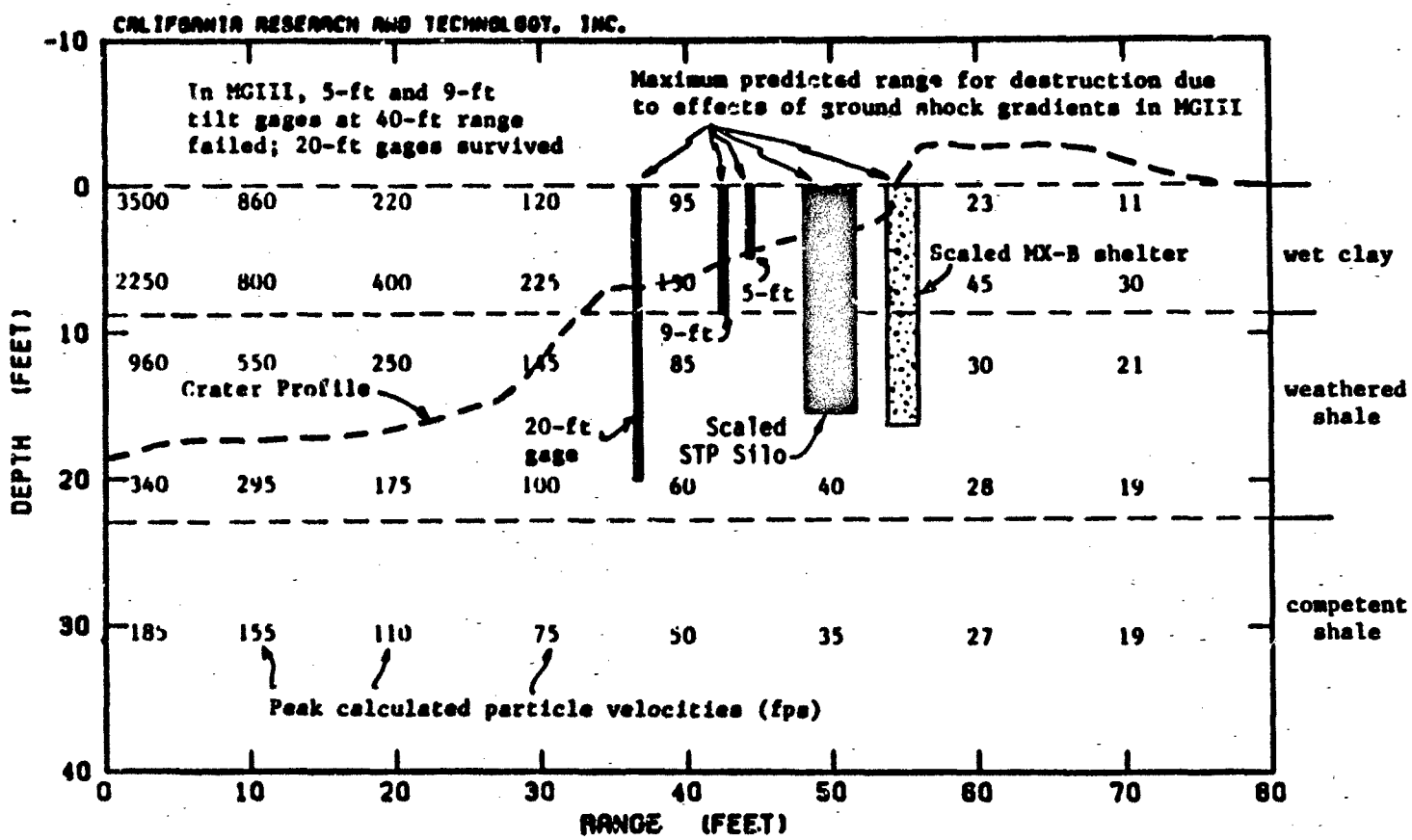

Figure 37. Maximum Predicted Range at which Tilt Gages and MX Vertical Shelter Model Will Be Destroyed Due to Effects of Ground Shock Gradients in MIDDLE GUST III.

5.3 Failure Due to Cratering Flow Displacement

Analysis: Quasi-Static

Model: Beam Structure with Soil Springs

Load: Free-Field Flow Displacement

Failure: Plastic Hinge

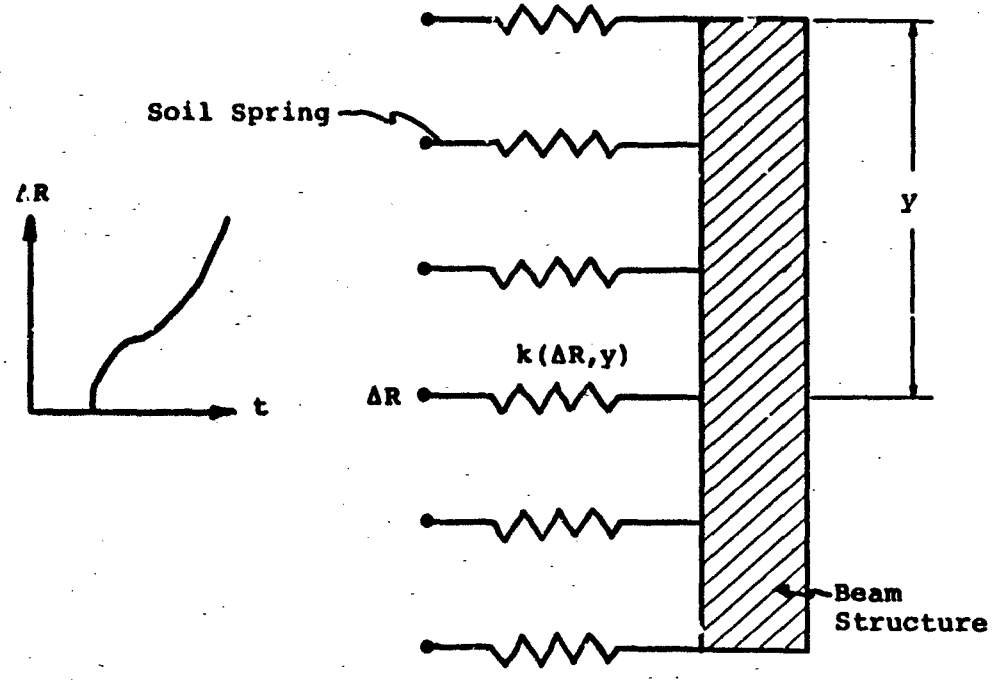

Figure 38. Failure Due to Cratering Flow Displacement.

- The late-time flow response of structures is evaluated using a quasi-static analysis procedure, wherein the prescribed free field flow displacements are input variables to the equivalent nonlinear soil springs. These nonlinear soil springs account for the soil/structure interaction loads on the structure which occur during the cratering event.

- Using this numerical approach, the response of scaled MX vertical structures at various ranges are determined based on the Middle Gust III Environment. That is, from the predetermined free field ground motions in Middle Gust III and from the appropriate equivalent nonlinear soil springs determined based on the Middle Gust material properties, the response of vertical and horizontal structures placed near the surface are analyzed.

- The rest of this section describes the procedures used to evaluate the equivalent nonlinear soil springs and the numerical response of various structures.

Evaluation of Structural Bending Response Due to Differential Free Field Displacements Along Structure

1. Late-time free field displacement histories are determined from finite difference analysis of cratering.

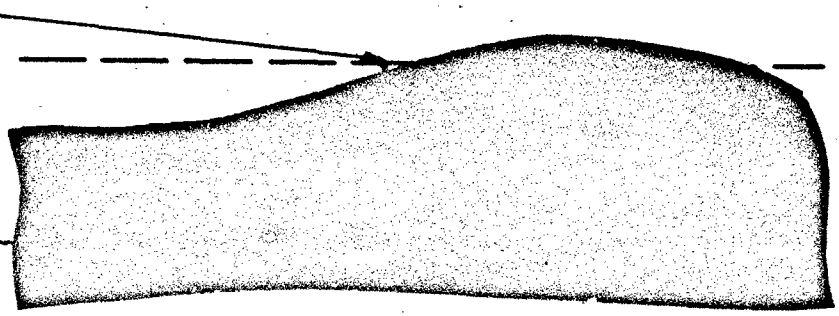

2. Late-time structural response is determined by applying prescribed free field displacements to structure model through non-linear soil springs.

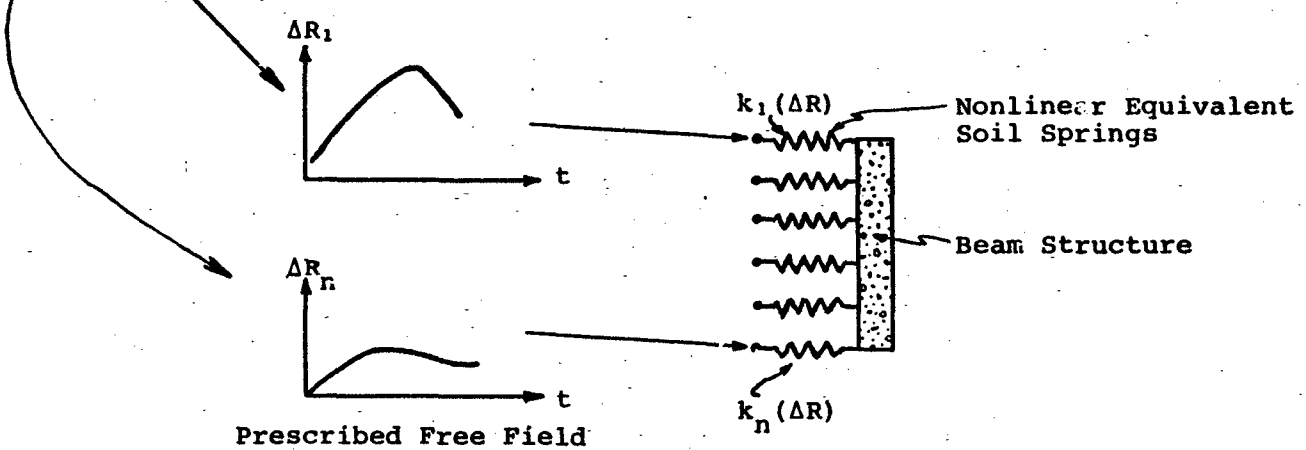

Figure 39. Evaluation of Structural Bending Response Due to Differential Free Field Displacements Along Structure.

- This figure shows the plane strain finite-element numerical model and describes the approach used to evaluate the equivalent non-linear soil springs. The constitutive model for the soil simulates both compaction as well as pressure dependent shear flow. Soil/structure interface is modeled using special interface elements which account for bonding/sliding and separation occurring between these materials using a coulomb-type sliding stress criterion and a nonassociated flow law. The concrete structure is modeled using an elastic assumption which in this example remains essentially rigid.

- The equivalent soil spring characteristics are determined by applying a monotonically increasing load to the rigid structure and determining its displacement from a static analysis.

- By evaluating the equivalent nonlinear soil springs for various geologies, the soil/structure interaction effects occurring for any cratering event can be evaluated using the analytical procedure described previously, provided the ground motions for the particular event are known.

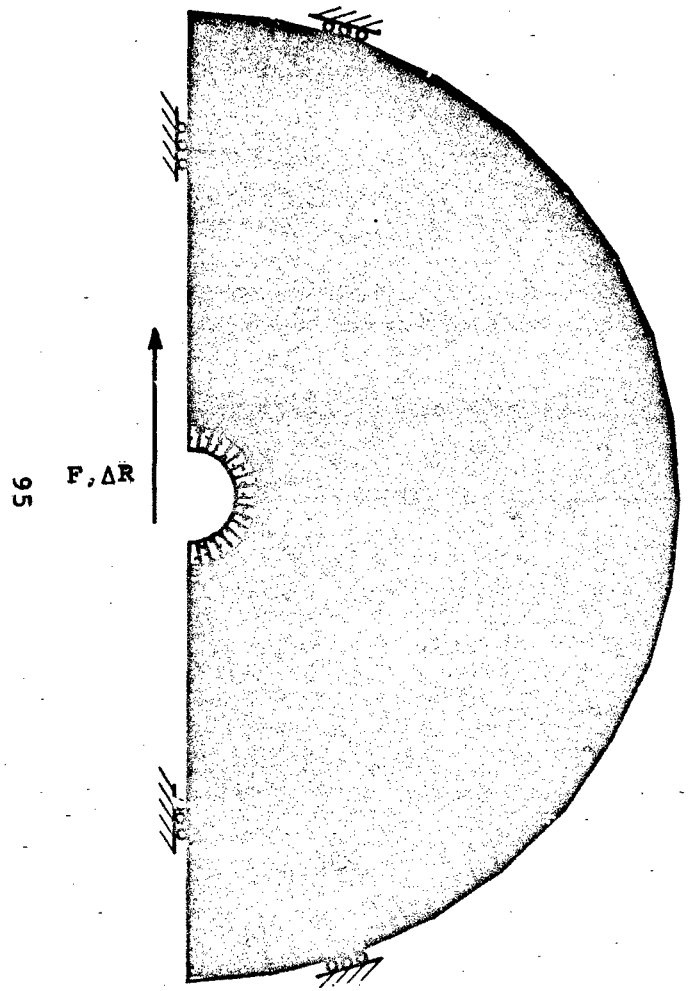

Plane Strain Finite Element Model Used to Evaluate Equivalent Soil Springs

- Rigid Structure
- Elastic-Plastic Soil Model
- SMI Elements used to Simulate Bonding, Slipping and Separation along Structure/Soil Interface

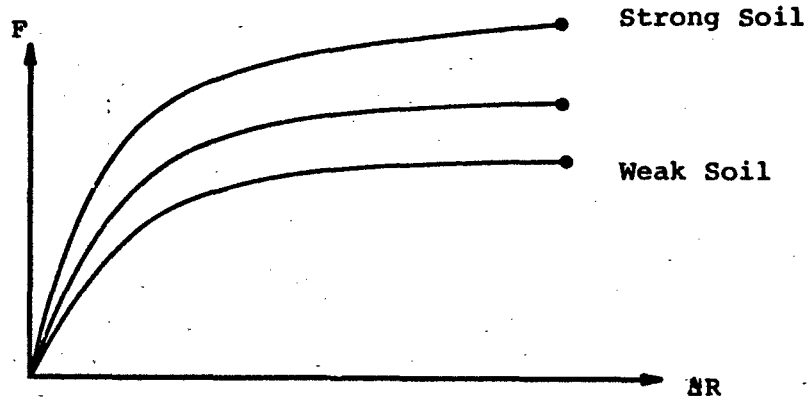

Typical Force-Displacement Relation Used to Evaluate Soil/Spring Parameters.

Figure 40. Plane Strain Finite Element Model Used to Evaluate Equivalent Soil Springs.

- This figure illustrates typical force/displacement characteristics of Middle Gust III geology determined from the finite-element approach on the previous figure. Two different equivalent soil springs were determined; one represents the nominal behavior of wet clay found from the ground surface to a depth of 9 feet. The other reflects the weathered shale found between the 9 to 23 ft depth.

- Using these nonlinear equivalent soil springs, and the numerical approach described earlier, the response of scaled MX vertical structures (16-ft long) placed near the surface in the Middle Gust III environment were evaluated. The vertical structures were subjected to free field motions determined from a finite difference numerical simulation of the Middle Gust crater.

- The remaining figures in this section describe the results of this numerical study.

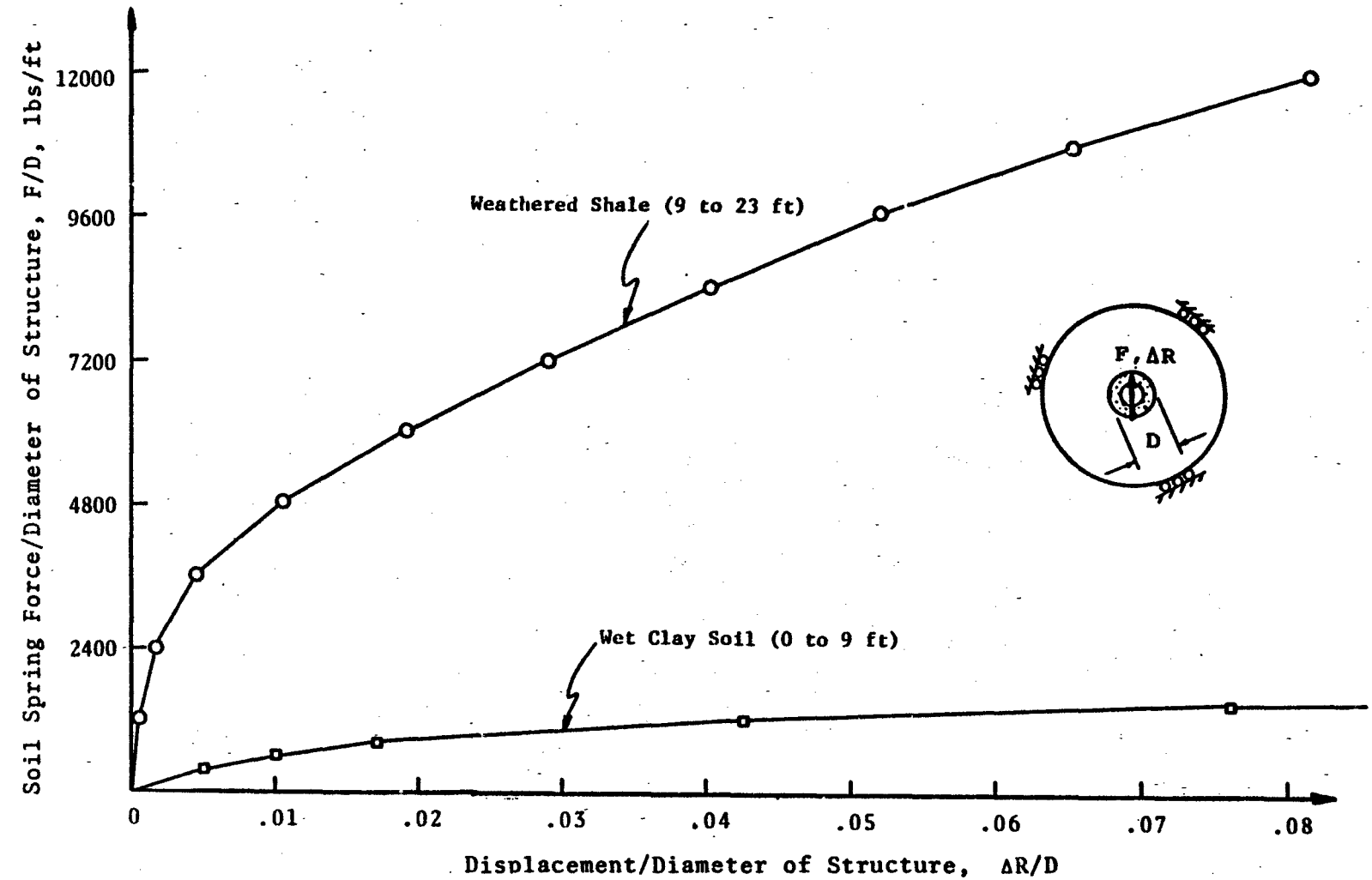

Figure 41. Nonlinear Soild Spring Force-Displacement Characteristics for Circular Cross-Section Structures, Based on Nominal Soil Properties (0-9 ft depth) and Weathered Shale Properties (9-23 ft depth) in MIDDLE GUST III Geology.

- This figure illustrates the typical interaction between the free soil and the deformable structure at the 40 ft range. Shown here are the initial undeformed structure, the late-time horizontal displacements of the free soil (at 200 msec) and of the structure. As indicated in this figure, the structure remains relatively undeformed and its motion consists of essentially rigid body translation and rotation. This figure also indicates the direction of soil/structure interaction loading, i.e , near the surface the radial motion of structure is greater than the free field soil: thus the interaction loading on the structure is directed toward ground zero. However, near the structure's mid-height the free field soil motion is greater than the structure, hence the interaction loading on the structure is directed away from ground zero. Finally, since the structure is in a state of static equilibrium, the interaction loads produce no resultant lateral force or moment.

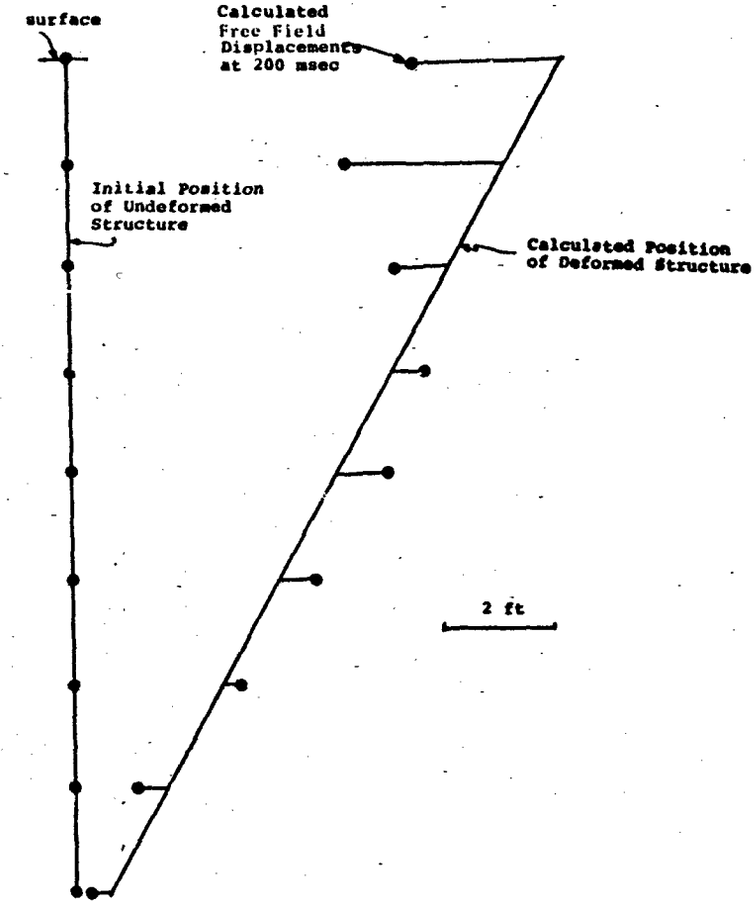

Horizontal Displacements of the Free Field at 40-ft Range in Middle Gust III at 200 msec, and of a Tilt Structure Model Assumed Located at that Range.

Figure 42. Horizontal Displacements of the Free Field at 40-ft Range in MIDDLE GUST III at 200 msec, and of a Tilt Structure Model Assumed Located at that Range.

- This figure compares the tilt angles determined by the foregoing method for steel tilt gage structures placed at the 40, 50, 60 and 80 ft range with values by tilt gages in the Middle Gust III experiment. The analytical values were determined based on free field displacement histories to 200 msec, while the experiment values are post-test measurements.

- The numerical results are in reasonably good agreement with experimental data and support the validity of the numerical approach.

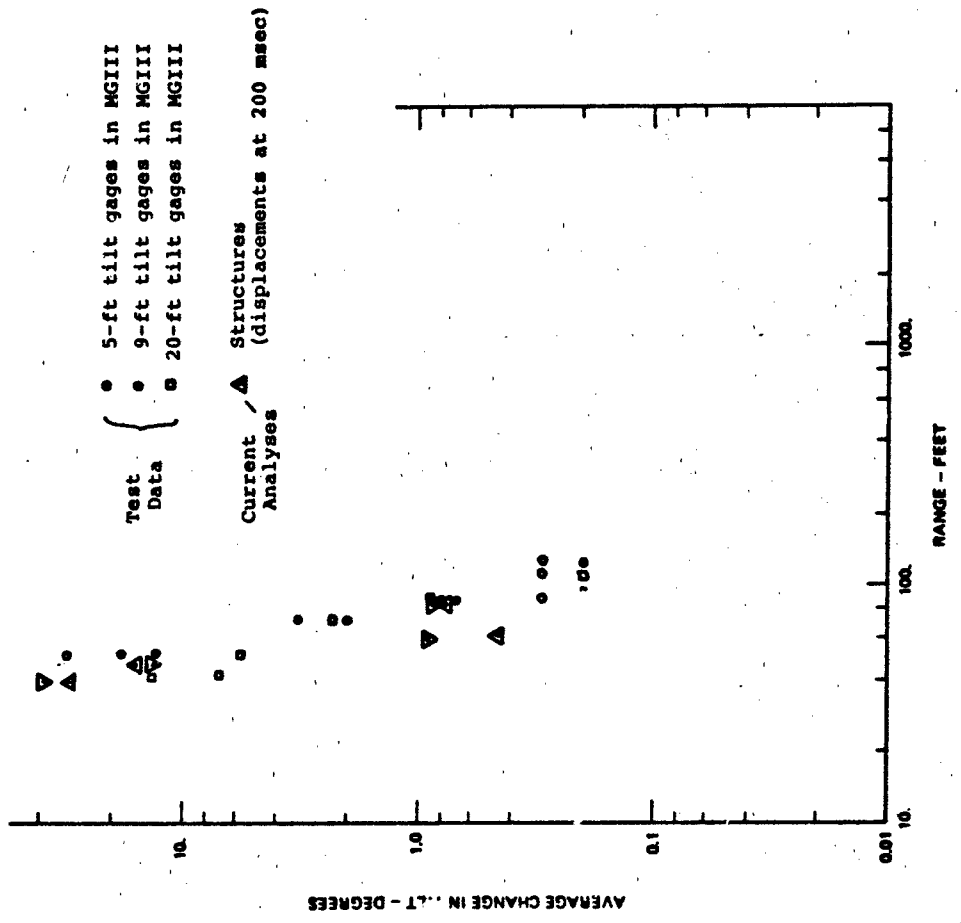

Figure 43. Comparison of Calculated Tilt of Vertical Structures with Tilt Gage Measurements in MIDDLE GUST III.

- This figure compares the peak bending stress determined in scaled vertical structures placed at various ranges in the Middle Gust III displacement field. These results clearly indicate a significant change in the peak bending stress occurring at about the 55 ft range, which corresponds with the calculated crater radius. These results imply that gross differences in structural response due to the late-time crater motions occur at the crater edge. Furthermore, based on typical confined compression limits of concrete, scaled MX-B vertical structures placed in the crater failed. Structures outside the crater remained elastic, however, the stress does not drop rapidly with increasing range.

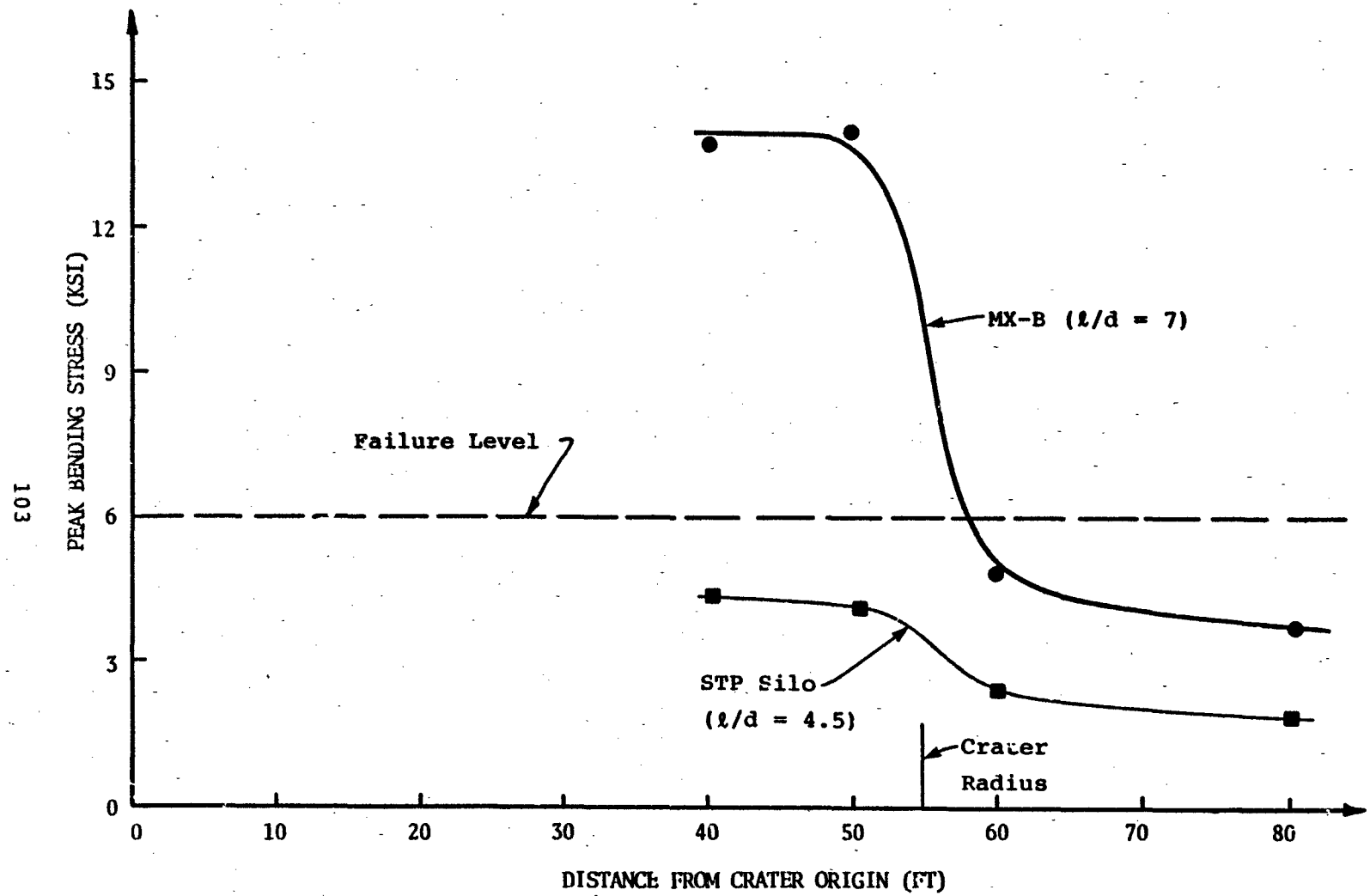

Figure 44. Peak Bending Stress in Scaled Vertical Structure Due to Differential Free Field Horizontal Displacements in MIDDLE GUST II Environment.

- This figure compares the peak bending stress distribution as a function of depth for the scaled MX-B vertical structures at various ranges in the Middle Gust III displacement field. At all but the largest range, the maximum bending stresses induced by crater ground motions occur near the clay-shale interface. The soil/structure interface loads for a given relative displacement are much larger in the shale than the clay; thus the structure is in essence cantilevered from the shale.

Peak Bending Stress Due to Differential Free Field Horizontal Displacements Along Scaled MX-B Vertical Structures Placed at Various Ranges in Middle Gust III Environment

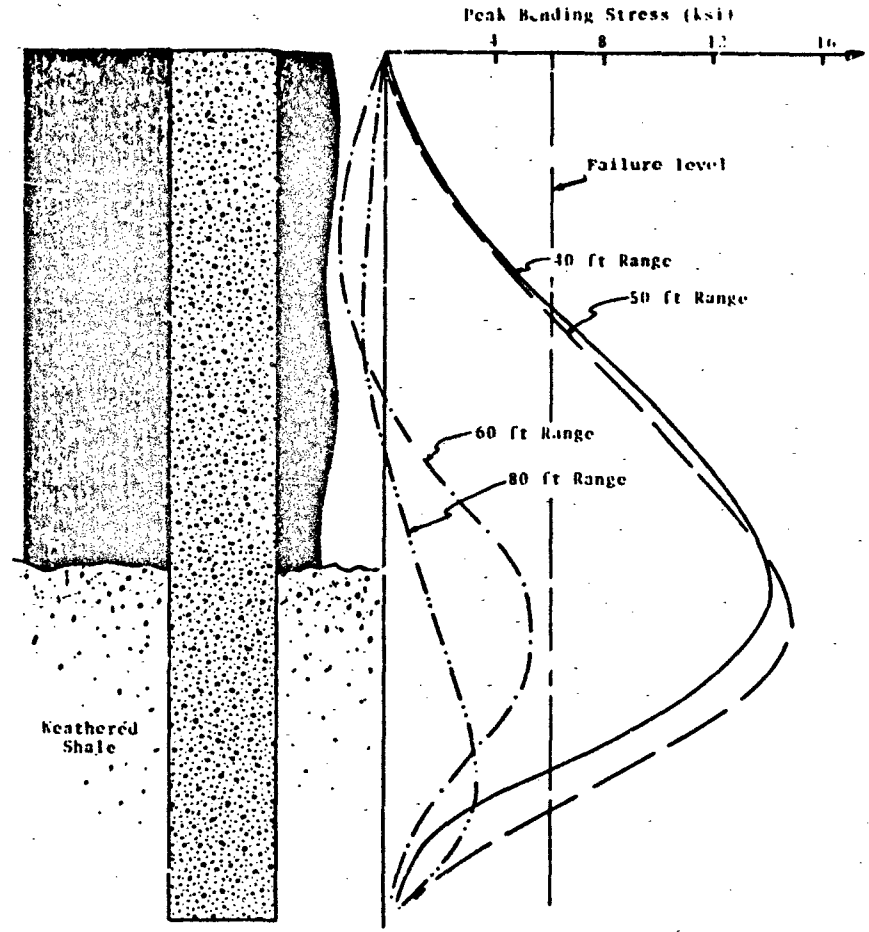

Figure 45. Peak Bending Stress Due to Differential Free Field Horizontal Displacements Along Scaled MX-B Vertical Structures Placed at Various Ranges in MIDDLE GUST III Environment.

- This plot compares the peak bending stress as a function of range determined for scaled MX-B structures placed horizontally near the surface (1 ft depth) in the Middle Gust III environment.

- The results of this analysis show behavior similar to that calculated for vertically placed structures. That is, a sharp transition in the peak bending stress occurs near the crater edge.

- Finally, it is noted that for a given range, horizontal structures in this environment would experience more displacement, but lower bending stresses than vertical structures. This is due to the shale which constrains the bottom of the vertical structures. Thus, the relatively strong shale produces high structure/soil interaction loads for small relative motions, whereas weak clay imparts smaller interaction loads for large soil/structure relative motions.

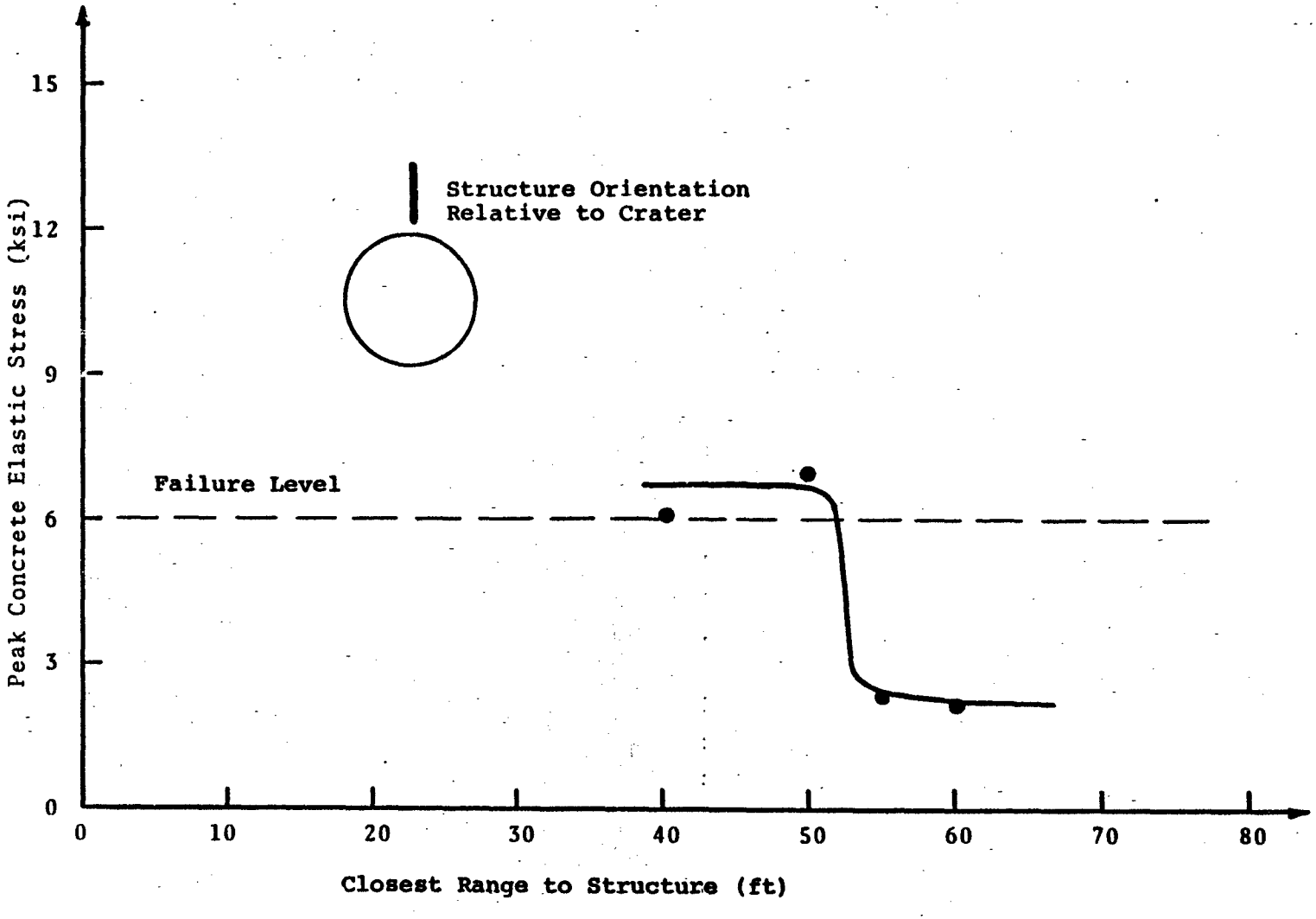

Figure 46. Peak Bending Stress Due to Differential Vertical Free Field Displacements Along Scaled MX-B Structure Placed Horizontally at 1-ft Depth in MIDDLE GUST III Environment.

SECTION 6

CONCLUSIONS AND RECOMMENDATIONS

Based on the results of this exploratory program, the following conclusions and recommendations are drawn.

CONCLUSIONS

- A practical methodology (finite-difference cratering code) exists for defining the dynamic environment in crater margins.

- A simplified procedure has been adopted (finite-element beam analysis with equivalent non-linear soil spring characteristics) for defining structure-media interactions in the large-displacement near-crater environment.

- Using simulated MIDDLE GUST III dynamic environment, response of representative structures (MX-B shelter and STP silo) at various ranges has been analyzed using simplified models. These structures are predicted to be destroyed out to the following maximum ranges due to decoupled effects of:

Environment	MX-B	STP
peak ground pressure (crushing failure)	55 ft	50 ft
dynamic ground shock gradient (plastic hinge failure)	58 ft	50 ft
late-time differential displacement (plastic hinge failure)	55 ft	<30 ft

These ranges are all in the crater (radius at 55 ft) margin.

- Distinct layering in the MIDDLE GUST III geology (probably typical of many target sites) substantially affects structure vulnerability to ground shock gradients and late-time differential displacements from cratering flow.

COMMENTS ON STRUCTURES EXPERIMENTS

- Environment near nuclear craters will be more severe than near HE craters, due to effects of 5-10 times higher peak overpressure at crater radius. Thus, HE sources alone (hemisphere of TNT or capped cylinder of ANFO) will not simulate the combined environment effects near nuclear craters.

- If test sites which are chosen have no strong reflective interface at a relatively shallow depth, the near-crater environment for model structures will probably not be as severe as for full-scale structures near nuclear craters in typical layered geologies.

- For structures testing, it would be desirable to select sites with representative scaled layering, and to field structure models both entirely within layers, and extending between layers.

- Box-type test structures will not be exposed to the high gradients within the crater margin and will essentially move as a rigid body with the media.

RECOMMENDATIONS

- Use environment defined by finite difference code analysis of nuclear benchmark crater in MIDDLE GUST III geology (current CRT calculation) to evaluate vulnerability of structures near nuclear crater.

- Use environment defined by prior calculations and test data from other HE tests to extend vulnerability analysis to structures near craters in other generic sites.

- Extend analysis methodology to include 3-D and coupled effects (e.g., superposition of shock crushing and shock gradient bending effects).

- Provide support analysis to near-crater structure experiment in MILL RACE HE event. This should include pre-test analysis of response of structures at various positions relative to crater rim, and participation in test planning and evaluation.

LIST OF REFERENCES

1. S. A. Kiger, Personal Communication on "Earth Penetrator (EP) Test," U.S. Army Engineer Waterways Experiment Station, February 1980.

2. B. L. Ristvet, E. L. Tremba, R. F. Couch, Jr., J. A. Fetzer, E. K. Cotey, D. R. Walter and V. P. Wendland, "Geologic and Geophysical Investigations of the Eniwetok Nuclear Craters," AFWL-TR-77-242, September 1978.

3. H. L. Brode, "Nuclear Craters on Bikini and Eniwetok Atolls: A Possible Explanation of the Disparity Between Theory and Observation," PSR Report 917, September 1979.

4. R. E. Crawford, C. J. Higgins and E. H. Bultmann, "The Air Force Manual for Design and Analysis of Hardened Structures," AFWL-TR-74-102, October 1974.

5. H. F. Cooper, Jr., "Estimates of Crater Dimensions for Near-Surface Explosions of Nuclear and High-Explosive Sources," RDA-TR-2604-001, September 1976.

6. "Instrumentation for Underground Explosion Test Program," Interim Technical Report No. 3, Engineering Research Associates, Inc., November 1951.

7. J. R. Hossley and G. E. Albritton, "ESSEX-DIAMOND ORE RESEARCH PROGRAM; Hardened Structure Response, Project ESSEX V," WES-TR-SL-79-11, November 1979.

8. J. R. Hossley, "ESSEX-DIAMOND ORE RESEARCH PROGRAM; ESSEX I, Phase 2: Structures Test," DNA PR 0020, November 1975.

9. G. K. Sinnamon, N. M. Newmark, R. E. Woodring and F. Matsuda, "Behavior of Underground Structures Subjected to an Underground Explosion, Operation Teapot," University of Illinois Report No. WE-1126, October 1957.

10. "Proceedings of the Mixed Company/Middle Gust Results Meeting 13-15 March 1973; Volume 1, Sessions 1, 2A and 3A," DNA 3151P, May 1973.

11. P. D. Smith and S. C. W. Ng, "Investigation of Buried Structures in Middle Gust Test Series, Volume I, Uninstrumented Structures," AFWL-TR-73-57 (Vol. I), April 1974.

12. R. J. Odello and C. R. Smith, "Silo Configuration Evaluation Test," DASA NA-007, October 1971.

13. L. E. Browder, "Structural Response of Unlined Vertical Cylinders in Granite to 100-Ton TNT Detonation," AFWL-TR-70-74, December 1970.

14. G. D. Jones and F. W. Davies, "Permanent Displacements in Rock: Operation Mine Shaft, Mine Ore Event," DASA 2276, May 1969,

15. B. L. Carnes, "An Analysis of Permanent Displacements Resulting from Surface or Near-Surface Explosions," MS Thesis, Mississippi State University, August 1974.

16. K. N. Kreyenhagen, "Some Problems in Past Cratering Calculations," DNA SPSS Biennial Review Conference, March 1979.

17. K. N. Kreyenhagen, "Review of Cratering Calculations," (in preparation).

18. G. Ialango, J. W. McDonald and J. B. Reid, "A Two-Dimensional Calculation of the Large Burst Phenomenoloy," DNA 3397F, August 1974.

19. D. L. Orphal, D. E. Maxwell, J. E. Reaugh and W. F. Borden, "A Computation of Cratering and Ground Motions from a 5 Mt Nuclear Surface Burst over a Layered Geology (ELK 76)," DNA 3711F, December 1975.

20. R. Swift, D. L. Orphal and W. F. Borden, "The Effect of Material Strength Degradation Cratering Dynamics (ELK 76-DEG)," DNA 4014F, May 1976.

21. K. N. Kreyenhagen and R. L. Bjork, "Analytical Study of Cratering in Alluvium," DASA 2459, March 1970.

22. P. T. Dzwilewski and G. W. Ullrich, "Numerical Simulations of Cratering and Ground Shocks from High Explosive and Nuclear Tests," AFWL-TR-79-2, May 1980.

23. S. A. Kiger, Personal Communication on "Shallow-Buried Structures Tests," U.S. Army Engineer Waterways Experiment Station, February 1980.

24. S. A. Kiger, "Static Test of a Hardened Shallow-Buried Structure," WES-TR-N-78-7, October 1978.

DISTRIBUTION LIST

DEPARTMENT OF DEFENSE

Defense Intelligence Agency
ATTN: DB-4C
ATTN: DB-4C, Rsch, Phys Vuln Br
ATTN: DB-4C2, C. Wiehle
ATTN: RTS-2B
ATTN: S. Halperson

Defense Nuclear Agency
ATTN: SPAS, G. Ullrich
ATTN: SPSS
4 cys ATTN: STTI-CA

Defense Technical Information Center
12 cys ATTN: DD

Field Command, Defense Nuclear Agency
ATTN: FCTT, W. Summa

Joint Strat Tgt Planning Staff
ATTN: JLK, DNA Rep
ATTN: JLKC
ATTN: JLKS
ATTN: JPPFN
ATTN: JPST

DEPARTMENT OF THE ARMY

US Army Engr Waterways Exper Station
ATTN: J. Ballard
ATTN: WESS, S. Kieger

US Army Nuclear & Chemical Agency
ATTN: MONA-OPS, B. Thomas
ATTN: MONA-OPS, J. Kelley

DEPARTMENT OF THE AIR FORCE

Air Force Weapons Laboratory
ATTN: NTE, M. Plamondon
ATTN: NTED, E. Seusy

Ballistic Missile Office/DAA
ATTN: ENSN

Foreign Technology Division
ATTN: SDBF, J. Vent

Strategic Air Command
ATTN: DOCSD
ATTN: DOM
ATTN: NRI/STINFO
ATTN: XPFR
ATTN: XPFS

DEPARTMENT OF DEFENSE CONTRACTORS

Aerospace Corp
ATTN: J. Crawford
ATTN: L. Selzer

DEPARTMENT OF DEFENSE CONTRACTORS (Continued)

Applied Research Associates, Inc
ATTN: D. Piepenburg

Applied Research Associates, Inc
ATTN: R. Frank

California Research & Technology, Inc
2 cys ATTN: K. Kreyhagen
2 cys ATTN: R. Ergland
2 cys ATTN: Y. Ito

California Research & Technology, Inc
ATTN: F. Sauer

H & H Consultants, Inc
ATTN: J. Haltiwanger
ATTN: W. Hall

Kaman Sciences Corp
ATTN: E. Conrad

Kaman Tempo
ATTN: DASIAC

Karagozian and Case
ATTN: J. Karagozian

Pacific-Sierra Research Corp
ATTN: H. Brode, Chairman SAGE

R & D Associates
ATTN: C. Lee
ATTN: C. Knowles
ATTN: D. Simons
ATTN: J. Lewis

R & D Associates
ATTN: G. Ganong

S-CUBED
ATTN: K. Pyatt

TRW Electronics & Defense Sector
ATTN: A. Feldman
ATTN: N. Lipner

Weidlinger Assoc, Consulting Engrg
ATTN: T. Deevy

Weidlinger Assoc, Consulting Engrg
ATTN: M. Baron

Weidlinger Assoc, Consulting Engrg
ATTN: J. Isenberg